Journal of Fluids and Structures (2001) **15,** 291–326
doi:10.1006/jfls.2000.0337, available online at http://www.idealibrary.com on IDEAL®

CONTROL OF FLOW PAST BLUFF BODIES USING ROTATING CONTROL CYLINDERS

S. MITTAL

Department of Aerospace Engineering, Indian Institute of Technology Kanpur, UP 208 016, India

(Received 31 May 1999, and in final form 11 July 2000)

Computational results for control of flow past a circular cylinder using small rotating cylinders are presented. A well-proven stabilized finite-element method, that has been applied to various flow problems earlier, is utilized to solve the incompressible Navier–Stokes equations in the primitive variables formulation. The formulation is first applied to study flow past an isolated rotating cylinder. Excellent match with experimental results, reported earlier, is observed. It is found that in purely two-dimensional flows, very high lift coefficients can be realized. However, it is observed, via three-dimensional Navier–Stokes simulations, that the end-effects and centrifugal instabilities along the cylinder span lead to a loss of lift and increase in drag. The aspect ratio of the cylinder plays an important role. The flow past a bluff body with two rotating control cylinders is studied using 2-D numerical simulations. The effect of the Reynolds number is studied by carrying out simulations for $\mathrm{Re} = 10^2$ and 10^4. Finite element meshes with an adequate number of grid points are employed to resolve the flow in the gap between the main and control cylinders. Two values of the gap are considered: $0{\cdot}01D$ and $0{\cdot}075D$, where D is the diameter of the main cylinder. It is observed that when the control cylinders rotate at high speed, such that the tip speed is 5 times the free-stream speed, the flow at $\mathrm{Re} = 100$ achieves a steady state. For $\mathrm{Re} = 10^4$, even though the flow remains unsteady, the wake is highly organized and narrower compared to the one without control. The results are in good agreement with the flow-visualization studies conducted by other researchers for bluff bodies using similar control concepts. In all the cases, a significant reduction in the overall drag coefficient and the unsteady aerodynamic forces acting on the main cylinder is observed. Results are also presented for the power requirements of the system for translation and rotation. It is found that the coefficient of power required for the rotation of control cylinders is significant for $\mathrm{Re} = 100$ but negligible for $\mathrm{Re} = 10^4$ flow. The size of the gap is found to be more critical for the $\mathrm{Re} = 10^4$ flows. This study brings out the relevance of the gap as a design parameter for such flow control devices.

1. INTRODUCTION

WIND-INDUCED FORCES, play an important role in the design of a variety of engineering structures. Control of vortex shedding leads to reduction in the unsteady forces acting on the bluff body and can significantly reduce its vibrations. Flow control may be accomplished by controlling the boundary layer separation and/or the structure of shear layer(s) in the wake.

Various methods, such as blowing, suction, surface roughness elements, etc., have been studied by researchers in the past. Review articles by Gad-el-Hak & Bushnell (1991), Griffin & Hall (1991) and Zdravkovich (1981) present a fairly comprehensive overview of the various means for suppressing vortex shedding. Zdravkovich (1981) presents control techniques that can be classified into three categories: surface protrusions, shrouds and near-wake stabilizers. He also investigated the relative effectiveness of the various means of flow

0889–9746/01/020291 + 36 $35.00/0

control by applying them to the same test model including the multi-cylinder arrangement. Griffin & Hall (1991) summarize the possible modification of the wake of a cylinder by its oscillatory motion. More details on the effect of the translational oscillations can be found in the work by Williamson & Roshko (1988), Ongoren & Rockwell (1988*a*, *b*), Lecointe *et al.* (1987), Mittal & Tezduyar (1992), and Mittal & Kumar (1999). Tokumaru & Dimotakis (1991, 1993) have demonstrated, via laboratory experiments, that a significant control on the structure of the wake can be achieved by subjecting the cylinder to rotary oscillations. In an effort to study a passive control device, Strykowski & Sreenivasan (1990) have reported that the vortex shedding past a circular cylinder can be controlled over a limited range of Reynolds number by the proper placement of a (smaller) control cylinder close to the main cylinder. Mittal & Raghuvanshi (2000) have verified the phenomenon using a numerical approach. They observed that the control cylinder provides a local favourable pressure gradient in the wake region, thereby stabilizing the shear layer locally. Gad-el-Hak & Bushnell (1991) review various techniques that are employed for separation control, including the moving-surface boundary layer control (MSBC) in which rotating cylinder elements are employed to inject momentum into the already existing boundary layer. Some ideas on these issues have been around for a fairly long time and have been presented by various authors, e.g. Goldstein (1938). He has reported the work carried out by Prandtl in 1907 who showed that by rotating a cylinder immersed in a stream of water he could prevent separation on the side advancing with the fluid. Modi *et al.* (1991*a*, *b*, 1992) and Munshi *et al.* (1997) have employed this concept to increase the maximum lift on airfoils and to reduce the drag on bluff bodies. Preliminary finite element simulations supporting these observations have been presented by Mittal (2000*a*, *b*). The degree of flow control depends on various parameters. Some of them include the number of control cylinders, their diameter relative to the characteristic dimension of the bluff body of interest, their speed of rotation and the gap between the bluff body and the control cylinder(s). Modi *et al.* (1991*a*, *b*, 2000) and Modi (1997) applied MSBC to two-dimensional airfoils in the subcritical range of Reynolds number ($\mathrm{Re} = 3 \times 10^4 - 5 \times 10^5$) with various arrangements of the control cylinders. Laboratory experiments were conducted for various angles of attack and rotation speeds of the control cylinders. The rotation speed of the control cylinder is characterized by the parameter U_c/U where U_c is the tip speed of the control cylinder and U is the free-stream speed of the flow. With $U_c/U = 4$ the stall angle goes up to 48° and the $C_{L,\max}$ goes up by as much as 210%. Flow visualization pictures confirm the delay of separation due to rotating control cylinders. Chew *et al.* (1998) have reported their numerical results for the effect of a moving wall on separation of flow past a symmetrical airfoil at Reynolds number $1{\cdot}43 \times 10^5$ based on chord-length. The optimal value of the lift-to-drag ratio (~ 60)is obtained at, approximately, an 8° angle of attack for $U_c/U = 4$.

Modi and his co-workers have applied the same concept to reduce drag and unsteady forces on bluff bodies; for example, Modi (1997), Modi *et al.* (1991, 1992, 2000), and Munshi *et al.* (1997*a*, *b*). The bluff bodies that they have studied include a flat plate at various angles of attack, rectangular prisms, D sections and tractor–trailer truck configurations. In all the cases, for high rotation rates of the control cylinders ($U_c/U \geq 4$), narrowing of the wake, delay of separation and a significant reduction in the drag is observed. The method has also been demonstrated to reduce flow-induced vibrations.

The most fundamental element of the control technique that is being investigated in this article is the flow past a rotating cylinder. Therefore, the first set of computations utilize the finite-element formulation to study the flow past an isolated spinning and translating cylinder. This problem has been studied by various researchers in the past. The results of Prandtl & Reid from laboratory experiments have been reported by Goldstein (1938). These include the effect of the aspect-ratio and end-plates attached to the end of a cylinder that

lead to an increase in the overall lift coefficient. Some of the later work on this flow problem includes the development of the near-wake behind an impulsively started cylinder via flow visualization by Coutanceau & Menard (1985). The time evolution of the vortices in the near-wake for a short time after the impulsive start comes out very clearly from their study. The highest Reynolds number in their study is less than 1000 and the rotation rate varies between 0 and 3·25. Badr & Dennis (1985) gave numerical solutions for the viscous flow equations for small rotation rates 0·5, 1·0 at $\mathrm{Re} = 200$ and 500, in which comparisons with experiments of Coutanceau & Menard (1985) have been made. Later, Badr *et al.* (1990) presented computational and experimental results for $\mathrm{Re} = 1000$ and rotation rates between 0·5 and 3. Excellent match was obtained between the two, except at high rotation rates where it is suspected that the experimental results show three-dimensional features. Computational results for the $\mathrm{Re} = 10^4$ flow were also presented. Tokumaru & Dimotakis (1991) demonstrated, via flow-visualization studies, that a considerable amount of control can be exerted over the structure of the wake by rotary oscillations of the cylinder. Later, they extended their study to measure the lift coefficient acting on rotating cylinders in Tokumaru & Dimotakis (1993). These motions include steady rotation and rotary oscillations with a net rotation rate. They have reported values of lift coefficient, from their laboratory experiments, that have exceeded the limit set by Goldstein (1938) based on the intuitive arguments given by Prandtl. According to Prandtl's arguments, the maximum value of the lift coefficient that can be achieved via Magnus effect is 4π ($\sim 12{\cdot}6$). For example, for $\mathrm{Re} = 3{\cdot}8 \times 10^3$ and $\alpha = 10$, Tokumaru & Dimotakis (1993) report an estimated lift coefficient that is more than 20% larger than this limit. This was observed for a cylinder with a span-to-diameter ratio of 18·7. Further, the trend of results that they have reported suggests that the value can be made larger for higher rotation rates and by taking cylinders of larger aspect ratio. They have suggested that perhaps it is the unsteady effects that weaken Prandtl's hypothesis and that the three-dimensional/end effects are responsible for lowering the value of lift coefficient that could be achieved in a purely two-dimensional flow. However, Chew *et al.* (1995) have reported that their computations are in agreement with Prandtl's postulate. They find that for $\mathrm{Re} = 1000$, the estimated mean lift coefficient approaches asymptotic values with increasing α. At $\alpha = 6$ they predict a mean lift coefficient of 9·1. In this sense, the present work assumes significance in contributing to the efforts of resolving the issue regarding the limit on maximum lift that is possible via the Magnus effect.

Computations for the $\mathrm{Re} = 1000$ flow and rotation rates of 0·5 and 2·0 lead to excellent agreement with the flow visualizations and computational studies carried out by other researchers, earlier. For a rotation rate of 3·0 the results from the present computations match very well with other computed results, reported earlier. However, the experimental results show certain differences, as compared to the 2-D computations, for larger times. This may be attributed to the 3-D nature of the flow. At high rotation rates it is seen that the lift for purely two-dimensional set-up can be very large. The values of the lift coefficient obtained in the present work exceed the maximum limit based on the arguments of Prandtl. It is also found, via computations in 3-D, that the aspect ratio of the cylinder (spanwise length/diameter) is an important parameter for the amount of lift generated by the rotating cylinder. The entire span is infected with centrifugal instabilities and, in addition, the end-effects cause separation of flow. Both these effects contribute to the loss of lift compared to that seen for a purely two-dimensional case. Good comparison between the 3-D computational results and the experimental results for the mean value of lift coefficient is seen.

In the present work, flow control past a circular cylinder using rotating control cylinders, of much smaller diameter, is studied numerically. None of the flow control studies, reported

to this date, have investigated the effect of the gap between the bluff body and control cylinders. The rotating control cylinders generate circulation and inject momentum from the outer flow into the wake of the main cylinder. It is expected that if the gap between the main and control cylinders is too large, then, even though the control cylinders rotating at high speeds may generate enough circulation, their effect on the main cylinders will be small. On the other hand, if the gap is too small, the interaction between the main and control cylinders will be large, but the control cylinders will not be able to generate significant circulation to achieve good flow control. Therefore, the gap is an important parameter in obtaining the optimal performance of the flow control system. One of the aims of the present study is to investigate the effect of gap on the control effectiveness. The effect of the Reynolds number on such flows is another point of interest of the present study. To this extent, computations are carried out at two values of gap (= 0·01D and 0·075D) and Reynolds numbers (100 and 10 000). Stabilized finite-element formulations are utilized to solve the viscous incompressible flow equations using primitive variables. The large-scale equation systems that result from the finite element discretization of the flow problem are solved using iterative solution techniques. The methods that are being used for the numerical simulations are well proven and have been used earlier to solve variety of flow problems. Some of the applications can be found in the articles by Mittal & Tezduyar (1995), Mittal & Kumar (1999) and Mittal *et al.* (1997). Detailed results, including time histories of the aerodynamic coefficients for forces acting on the bodies and power required, are presented.

The outline of the rest of the article is as follows. We begin by reviewing the governing equations for incompressible fluid flow in Section 2. The streamline-upwind/Petrov–Galerkin (SUPG) and pressure-stabilizing/Petrov–Galerkin (PSPG) stabilization technique is employed to stabilize our computations against spurious numerical oscillations and to enable us to use equal-order-interpolation velocity–pressure elements. More details on these techniques can be found in the articles by Tezduyar *et al.* (1992), Hughes & Brooks (1979) and Hughes & Tezduyar (1984). Section 3 describes the finite-element formulation incorporating these stabilizing terms. In Section 4, computational results for flows involving the main and control cylinders are presented and discussed. In Section 5, the results are summarized and a few concluding remarks are made.

2. THE GOVERNING EQUATIONS

Let $\Omega \subset \mathbb{R}^{n_{sd}}$ and $(0, T)$ be the spatial and temporal domains, respectively, where n_{sd} is the number of space dimensions, and let Γ denote the boundary of Ω. The spatial and temporal coordinates are denoted by $\mathbf{x}$ and t. The Navier–Stokes equations governing incompressible fluid flow are

$$\rho\left(\frac{\partial \mathbf{u}}{\partial t} + \mathbf{u}\cdot\nabla\mathbf{u} - \mathbf{f}\right) - \nabla\cdot\boldsymbol{\sigma} = \mathbf{0} \quad \text{on } \Omega \text{ for } (0, T), \tag{1}$$

$$\nabla\cdot\mathbf{u} = \mathbf{0} \quad \text{on } \Omega \text{ for } (0, T). \tag{2}$$

Here ρ, $\mathbf{u}$, $\mathbf{f}$ and $\boldsymbol{\sigma}$ are the density, velocity, body force and the stress tensor, respectively. The stress tensor is written as the sum of its isotropic and deviatoric parts:

$$\boldsymbol{\sigma} = -p\mathbf{I} + \mathbf{T}, \quad \mathbf{T} = 2\mu\boldsymbol{\varepsilon}(\mathbf{u}), \quad \boldsymbol{\varepsilon}(\mathbf{u}) = \tfrac{1}{2}((\nabla\mathbf{u}) + (\nabla\mathbf{u})^{\mathrm{T}}), \tag{3}$$

where p and μ are the pressure and coefficient of dynamic viscosity. Both the Dirichlet and Neumann-type boundary conditions are accounted for, represented as

$$\mathbf{u} = \mathbf{g} \text{ on } \Gamma_g, \quad \mathbf{n}\cdot\boldsymbol{\sigma} = \mathbf{h} \text{ on } \Gamma_h, \tag{4}$$

where Γ_g and Γ_h are complementary subsets of the boundary Γ. The initial condition on the velocity is specified on Ω:

$$\mathbf{u}(\mathbf{x}, 0) = \mathbf{u}_0 \quad \text{on } \Omega, \tag{5}$$

where $\mathbf{u}_0$ is divergence free.

The force and moment coefficients are computed by carrying an integration, that involves the pressure and viscous stresses, around the circumference of the solid body (in this case, cylinders):

$$C_D = \frac{1}{(1/2)\rho U^2 2a} \int_{\Gamma_{\text{cyl}}} (\boldsymbol{\sigma}\mathbf{n}) \cdot \mathbf{n}_x \, \mathrm{d}\Gamma, \tag{6}$$

$$C_L = \frac{1}{(1/2)\rho U^2 2a} \int_{\Gamma_{\text{cyl}}} (\boldsymbol{\sigma}\mathbf{n}) \cdot \mathbf{n}_y \, \mathrm{d}\Gamma, \tag{7}$$

$$C_M = \frac{1}{(1/2)\rho U^2 2a^2} \int_{\Gamma_{\text{cyl}}} (\boldsymbol{\sigma}\mathbf{n}) \times (\mathbf{r} - \mathbf{r}_0) \, \mathrm{d}\Gamma. \tag{8}$$

Here $\mathbf{n}_x$ and $\mathbf{n}_y$ are the Cartesian components of the unit vector $\mathbf{n}$ that is normal to the cylinder boundary Γ_{cyl}, a is the radius of the main cylinder, $\mathbf{r}$ is the position vector of a point lying on the cylinder surface, $\mathbf{r}_0$ is the location of the centre of the cylinder, and U the free-stream speed. C_D, C_L and C_M represent the drag, lift and moment coefficient, respectively. The contribution of the drag to the power coefficient (C_P) is C_D and that of the moment coefficient is $C_M \omega a/U$ where, ω is the rate of rotation of the cylinder. All the results presented in this article are with respect to the nondimensional time $\tau = Ut/a$, where t is the actual time.

3. FINITE-ELEMENT FORMULATION

Consider a finite-element discretization of Ω into subdomains Ω^e, $e = 1,2,\ldots,n_{\text{el}}$, where n_{el} is the number of elements. Based on this discretization, for velocity and pressure we define the finite-element trial function spaces $\mathscr{S}_{\mathbf{u}}^h$ and $\mathscr{S}_p^h$, and weighting function spaces $\mathscr{V}_{\mathbf{u}}^h$ and $\mathscr{V}_p^h$. These function spaces are selected, by taking the Dirichlet boundary conditions into account, as subsets of $[\mathbf{H}^{1h}(\Omega)]^{n_{sd}}$ and $\mathbf{H}^{1h}(\Omega)$, where $\mathbf{H}^{1h}(\Omega)$ is the finite-dimensional function space over Ω. The stabilized finite-element formulation of equations (1) and (2) is written as follows: find $\mathbf{u}^h \in \mathscr{S}_{\mathbf{u}}^h$ and $p^h \in \mathscr{S}_p^h$ such that $\forall \mathbf{w}^h \in \mathscr{V}_{\mathbf{u}}^h$, $q^h \in \mathscr{V}_p^h$

$$\begin{aligned}
&\int_\Omega \mathbf{w}^h \cdot \rho \left(\frac{\partial \mathbf{u}^h}{\partial t} + \mathbf{u}^h \cdot \nabla \mathbf{u}^h - \mathbf{f} \right) \mathrm{d}\Omega + \int_\Omega \boldsymbol{\varepsilon}(\mathbf{w}^h) : \boldsymbol{\sigma}(p^h, \mathbf{u}^h) \, \mathrm{d}\Omega + \int_\Omega q^h \nabla \cdot \mathbf{u}^h \, \mathrm{d}\Omega \\
&\quad + \sum_{e=1}^{n_{\text{el}}} \int_{\Omega^e} \frac{1}{\rho} (\tau_{\text{SUPG}} \rho \mathbf{u}^h \cdot \nabla \mathbf{w}^h + \tau_{\text{PSPG}} \nabla q^h) \cdot \\
&\left[\rho \left(\frac{\partial \mathbf{u}^h}{\partial t} + \mathbf{u}^h \cdot \nabla \mathbf{u}^h - \mathbf{f} \right) - \nabla \cdot \boldsymbol{\sigma}(p^h, \mathbf{u}^h) \right] \mathrm{d}\Omega^e \\
&\quad + \sum_{e=1}^{n_{\text{el}}} \int_{\Omega^e} \delta \nabla \cdot \mathbf{w}^h \rho \nabla \cdot \mathbf{u}^h \, \mathrm{d}\Omega^e = \int_{\Gamma_h} \mathbf{w}^h \cdot \mathbf{h}^h \, \mathrm{d}\Gamma.
\end{aligned} \tag{9}$$

In the variational formulation given by equation (9), the first three terms and the right-hand-side constitute the Galerkin formulation of the problem. It is well known that

the Galerkin formulation is unstable with respect to the advection operator as the cell Reynolds number (based on the local flow velocity and mesh size) becomes larger. Also, not all combinations of the velocity and pressure interpolations are admissible to the Galerkin formulation. Elements that do not satisfy the Babuska–Brezzi condition lead to oscillatory solutions and, sometimes, no solution at all. To render stability to the basic formulation, a series of element-level integrals are added. The first series of element-level integrals are the SUPG and PSPG stabilization terms added to the variational formulations as described by Tezduyar *et al.* (1992) and Mittal (1992). The terms with τ_{SUPG} as the coefficient render stability to the formulation in the presence of advection operator. The term involving τ_{PSPG} allows one to use any combination of velocity and pressure interpolation, including equal-order interpolation. In the current formulation τ_{PSPG} is the same as τ_{SUPG} and is given as

$$\tau = \left(\left(\frac{2\|\mathbf{u}^h\|}{h} \right)^2 + \left(\frac{12\nu}{h^2} \right)^2 \right)^{-1/2} \tag{10}$$

The second series of element-level integrals are added to the formulation for numerical stability at high Reynolds numbers. This is a least-squares term based on the continuity equation. The coefficient δ is defined as

$$\delta = \frac{h}{2} \|\mathbf{u}^h\| z, \tag{11}$$

where

$$z = \begin{cases} (\frac{1}{3} Re_u) & \mathrm{Re}_u \leq 3, \\ 1 & \mathrm{Re}_u > 3 \end{cases} \tag{12}$$

and Re_u is the cell Reynolds number. Both stabilization terms are weighted residuals, and therefore maintain the consistency of the formulation; h is the *element length*, and various definitions have been used by researchers in the past. Mittal (2000*a*, *b*) conducted a systematic numerical study to investigate the effect of high aspect ratio elements on the performance of the finite-element formulation for three commonly used definitions of h. The one which results in the least sensitivity of the computed flow to the element aspect ratio has been used for computations in the present work. According to this definition, the element length is equal to the minimum edge length of a triangular (three-noded) element. More details on the finite-element formulation can be found in the article by Tezduyar *et al.* (1992). The error-estimates for the stabilized finite-element method as applied to the advective–diffusive model can be found in the paper by Franca *et al.* (1992). The analysis for the formulation as applied to the incompressible Navier–Stokes equations and the generalization of the method to higher order equal-order-interpolation elements can be found in the work by Franca & Frey (1992). The interested reader can also refer to the work by Shakib & Hughes (1991) for the Fourier stability and accuracy analysis of this class of methods, both, in the context of space–time and semidiscrete formulations.

4. NUMERICAL SIMULATIONS

All the computations reported in this article are carried out on the Digital and Silicon-Graphics work-stations at IIT Kanpur in 64-bit precision. Equal-in-order interpolation functions for velocity and pressure have been employed. With the P1P1 element that is

based on the linear basis functions, a 3-point quadrature is employed for numerical integration while a 2×2 point quadrature is utilized with the Q1Q1 elements based on bi-linear basis functions. The non-linear equation systems resulting from the finite-element discretization of the flow equations are solved using the Generalized Minimal RESidual (GMRES) technique (see Saad & Schultz 1986) in conjunction with diagonal preconditioners.

4.1. Flow Past an Isolated Rotating Cylinder

The heart of the flow control technique being studied in the present work is the flow past a rotating cylinder. Flow past a translating and rotating cylinder has been a subject of extensive study and several researchers have contributed to the understanding of the flow. The Reynolds number is defined as $\mathrm{Re} = 2Ua/v$ where a is the radius of cylinder, U the free-stream speed (after an impulsive start) and v is the coefficient of kinematic viscosity of the fluid. The rotation rate of the cylinder is nondimensionalized with respect to the free-stream speed and is given as $\alpha = a\omega/U$, where ω is the angular velocity of the cylinder about its own axis. Most of the computations reported earlier, for this flow problem, have been carried out using the vorticity/stream-function formulations, for example, by Badr *et al.* (1990) and Chew *et al.* (1995) or with the vorticity/velocity formulations as by Chen *et al.* (1993). The present effort employs the finite-element formulation of the Navier–Stokes equations in the primitive variables. The cylinder resides in a rectangular domain and a flow velocity corresponding to the rotation-rate, α is specified on the cylinder surface. Free-stream value is assigned for the velocity at the upstream boundary while at the downstream boundary, a Neumann-type boundary condition for the velocity is specified that corresponds to zero viscous stress vector. On the upper and lower boundaries, the component of velocity normal to and the component of stress vector along these boundaries is prescribed zero value.

Figure 1 shows the results for the computation of $\mathrm{Re} = 10^3$ flow past a cylinder with $\alpha = 0{\cdot}5$ with an impulsive start. Also shown in the figure are the computational and experimental results from Badr *et al.* (1990). The computations have been carried out with a mesh containing 12 408 nodes and 12 176 quadrilateral elements. All the external boundaries are located at eight cylinder diameters from the cylinder centre. The time step for the computations is 0·01. It can be observed from the figure that the present computations reproduce all the essential features of the flow and their time evolution. It should be mentioned that the instantaneous streamlines, shown in the figure, have been derived from the computed velocity field via a least-squares procedure. The results for $\mathrm{Re} = 1000$ and $\alpha = 2{,}3$ have also been computed and compared with those from Badr *et al.* (1990). In all the cases, except at $t = 4$ and 6 for $\alpha = 3$, excellent agreement with the flow visualization results of Badr *et al.* (1990) is observed. For $\alpha = 3$, the computational results of Badr *et al.* (1990) and the present results match quite well but there is some difference between the experimental results and those obtained from computations. The vortex on the windward side of the cylinder appears to be more fuzzy and located at a smaller angle with the free-stream direction for the experimental results. This discrepancy is perhaps because of the three-dimensional effects that have been neglected in the two-dimensional computations. Chew *et al.* (1995) have also reported their numerical results for the same set of parameters and their results are in close agreement with the computational results of Badr *et al.* and the present ones. The difference between the experimental and computational results is more pronounced for $t = 6$ as compared to that at $t = 4$. As will be seen later in this section, after an impulsive start the flow remains two-dimensional for some time, and then the three-dimensional effects develop. The excellent match between the results from the present

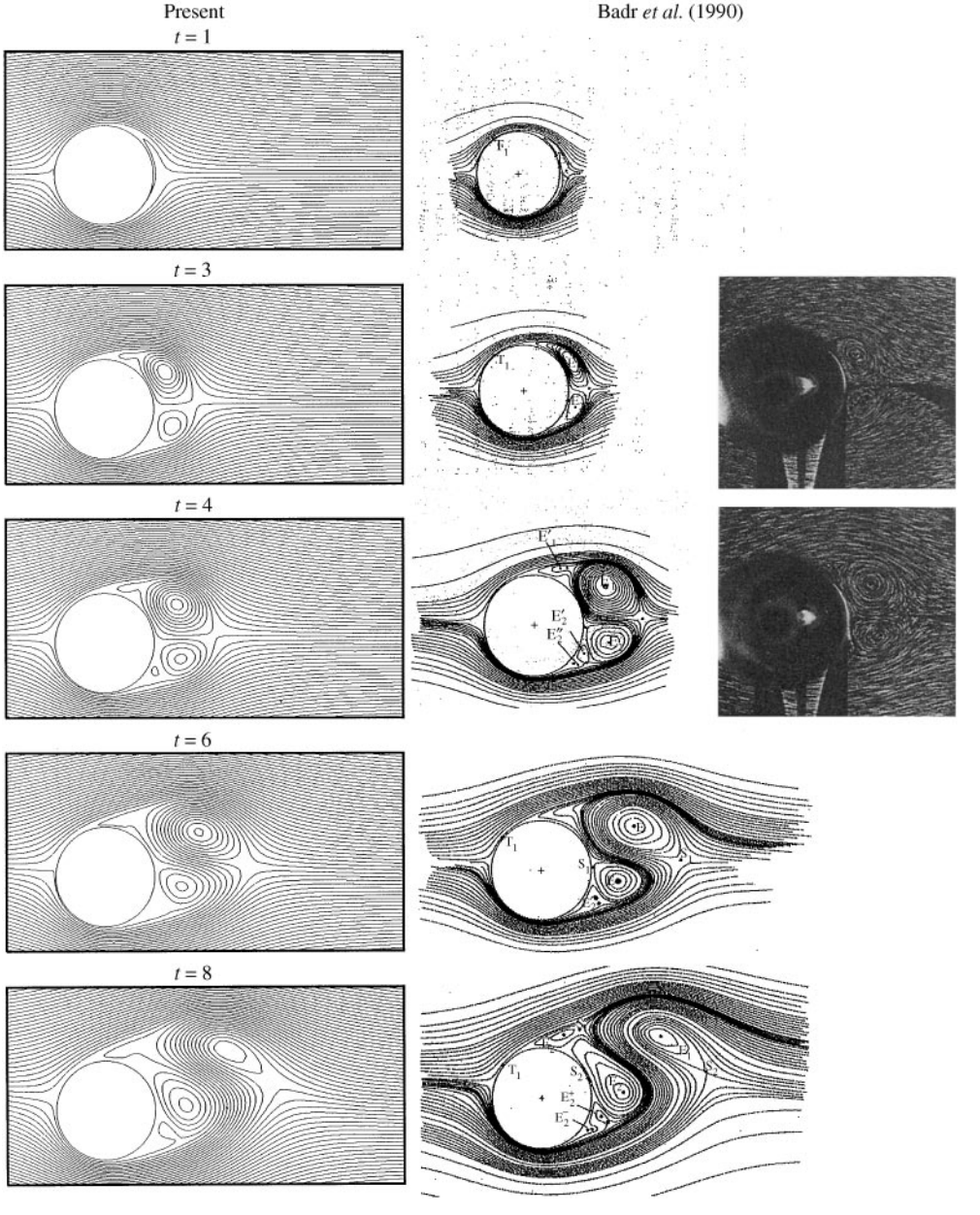

Figure 1. $\mathrm{Re} = 10^3$, $\alpha = 0{\cdot}5$ flow past a rotating cylinder: comparison of the instantaneous streamline patterns at various time instants from the present computations and those from Badr *et al.* (1990).

computations and those from other researchers increase our confidence in the present formulation in computing flows that involve rotating cylinders.

The next set of results are presented for $\mathrm{Re} = 5$ and $\alpha = 5$. During the entire simulation, only one clockwise vortex (the start-up vortex) is shed from the rotating cylinder. A set of closed streamlines form around the rotating cylinder. In this computation, the finite-element mesh consists of 12 678 nodes and four-noded quadrilateral 12 420 elements. The mesh is fine enough to resolve the boundary layer and other flow features, adequately, for

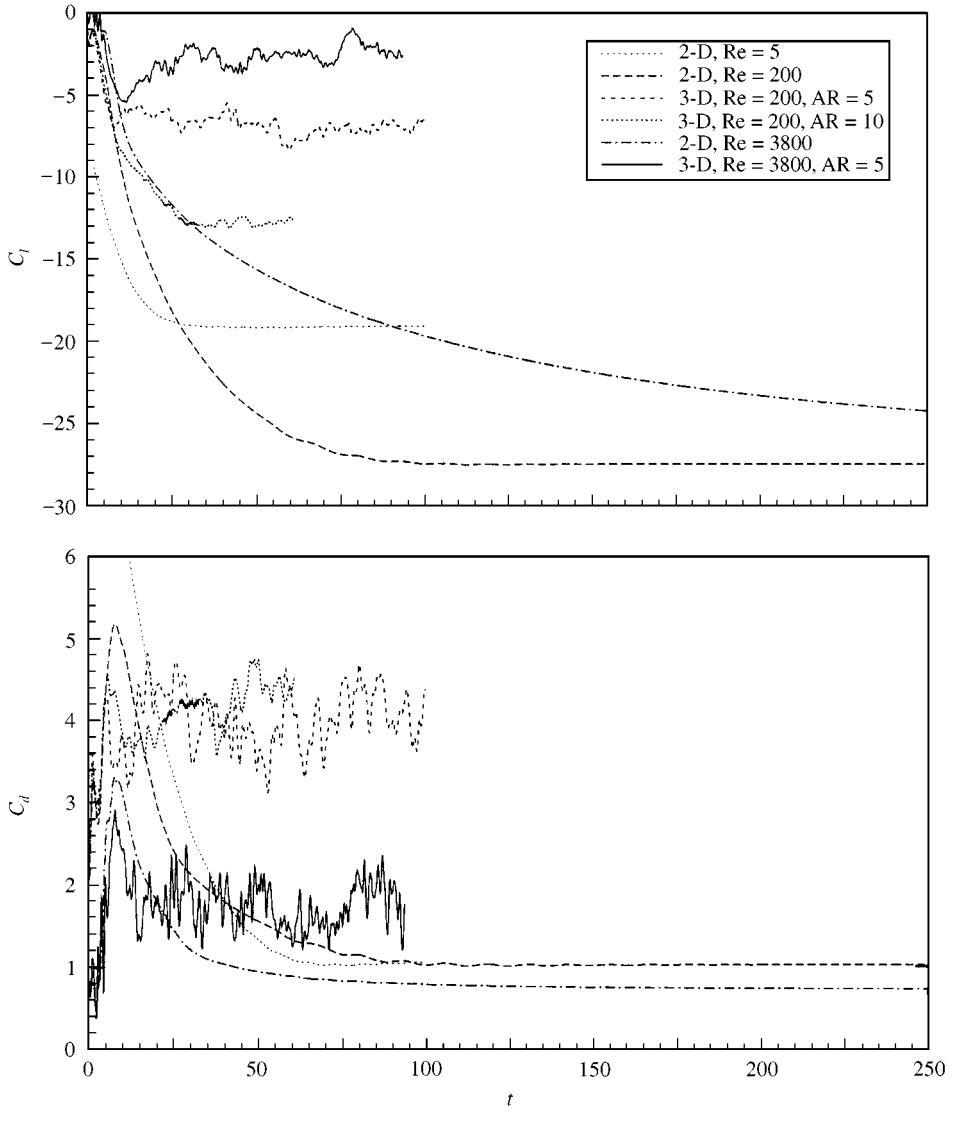

Figure 2. Re = 5, 200, and 3800, $\alpha = 5{\cdot}0$ flow past a rotating cylinder: time histories of the lift and drag coefficient for two- and three- dimensional computations.

this low Reynolds number. The external boundaries are located at 25 cylinder diameters from the centre of the cylinder. Computations with a domain with the boundaries located at 20 cylinder diameters from the cylinder result in an almost indistinguishable solution. The time histories of the lift and the drag coefficients from the simulation are shown in Figure 2. Note that the steady-state lift coefficient obtained from the present simulation is 19·1. This value is much larger than the limit set by Goldstein (1938) based on intuitive arguments by Prandtl. According to his arguments, the maximum value of the lift coefficient that can be achieved via the Magnus effect is 4π ($\sim 12{\cdot}6$). This issue has still not been resolved and one can find papers in the literature that support and others that do not agree with the limit on the maximum value of the lift coefficient. For example, Chew *et al.* (1995) have reported that their computations are in agreement with Prandtl's postulate. They find that for Re = 1000

the estimated mean lift coefficient approaches asymptotic values with increase in α. At $\alpha = 6$ they predict a mean lift coefficient of 9·1. However, Tokumaro & Dimotakis (1993) have reported values of lift coefficient, from their laboratory experiments, that have exceeded this limit. For example, for $\mathrm{Re} = 3{\cdot}8 \times 10^3$ and $\alpha = 10$, they report an estimated lift coefficient that is more than 20% larger than the proposed upper limit by Prandtl. This was observed for a cylinder with a span-to-diameter ratio of 18·7. Further, the trend of results that they have reported suggests that the value can be made larger for higher rotation rates and by taking cylinders of larger aspect ratio. They have suggested that perhaps it is the unsteady effects that weaken Prandtl's hypothesis and that the three-dimensional/end effects are responsible for lowering the value of lift coefficient that could be achieved in a purely two-dimensional flow. Recall that the potential flow theory predicts a C_L value of $2\pi\alpha$ which is, approximately, 31·4 for $\alpha = 5$. In view of this, it is interesting to observe from our computed results that, as t increases, the streamline pattern around the circular cylinder approaches the one that is observed for potential flows. Figure 2 also shows the time histories of the lift and drag coefficients for $\mathrm{Re} = 200$ and $\alpha = 5$. For this case, the steady-state lift coefficient for the two-dimensional computation is 27·5. This value is even closer to that suggested by the potential flow theory. This suggests that for the purely two-dimensional flows, at least for low Reynolds numbers, one can expect high values of lift coefficients that exceed the limit set by Prandtl.

Tokumaro & Dimotakis (1993) have reported a strong dependence of the lift coefficient on the aspect ratio of the cylinder and its end-conditions. To study the same, we carried out three-dimensional computations for flow past a rotating cylinder with impulsive start for two values of the axial length of the cylinder. In the three-dimensional simulations, one of the side boundaries is assumed to be a no-slip wall while symmetry conditions are imposed on the other side wall. These boundary conditions simulate a rotating cylinder, without end-plates, placed in a tunnel. Only one-half of the tunnel is being simulated. The first simulation is with a cylinder of aspect ratio (span-wise length/cylinder diameter) $AR = 5$, while the other with AR = 10. The time histories of the lift and drag coefficients for these simulations are shown in Figure 2 along with the results from the two-dimensional computations. Our 3-D computations reveal that the interaction of the rotating cylinder with the boundary layer on the "no-slip" wall leads to flow separation. In addition, the entire span of the cylinder is infected with centrifugal instabilities such as those observed in flow between two concentric cylinders. Both these effects contribute to a loss in the lift. As can be observed from Figure 2, the AR of the cylinder has a very significant effect on the magnitude of lift generated by the rotating cylinder. As pointed out by Tokumaro & Dimotakis (1993) the present computations also suggest that the lift coefficient can be made larger by increasing the aspect ratio of the cylinder. The trend in Figure 2 suggests that it is possible to exceed the limit proposed by Prandtl for the maximum value of lift coefficient. It can also be noticed from the figure that the drag coefficient for the three-dimensional case is substantially higher than that for the 2-D computations. The results for $\mathrm{Re} = 3800$ for $\alpha = 5$ are also shown in Figure 2 and are consistent with the observations for $\mathrm{Re} = 200$.

The final set of results, presented in this subsection, for flow past an isolated rotating cylinder are for $\mathrm{Re} = 3{\cdot}8 \times 10^3$ and $\alpha = 2$. These parameters have been chosen based on the results presented by Tokumaro & Dimotakis (1993). The results from 2-D computations for this case have been reported in the work by Mittal *et al.* (1997) using the finite element and finite difference methods. The two methods result in almost identical solution to this particular case of flow problem. The time histories of the lift and drag coefficients with the finite-element method is shown in Figure 3. The mean lift coefficient from the 2-D computations is, approximately, 5·5. The mean lift coefficient reported by Chew *et al.* (1995)

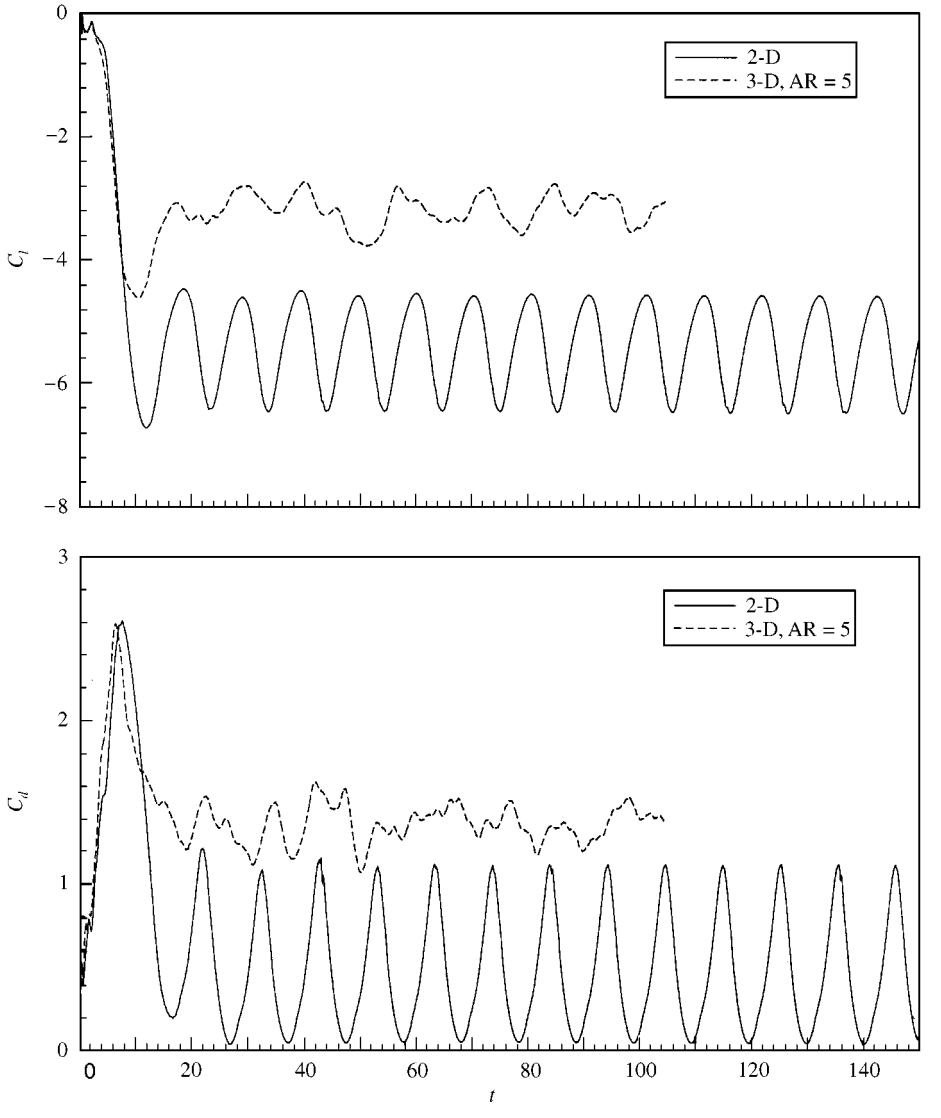

Figure 3. $\mathrm{Re} = 3{\cdot}8 \times 10^3$, $\alpha = 2{\cdot}0$ flow past a rotating cylinder: time histories of the lift and drag coefficient for two- and three-dimensional computations.

for $\mathrm{Re} = 1000$ and same value of α ($= 2$) is 5·81. Tokumaro & Dimotakis (1993) report a value of, approximately, 4 for a cylinder of $\mathrm{AR} = 18{\cdot}7$ and at $\mathrm{Re} = 3{\cdot}8 \times 10^3$. This points to a significant discrepancy between the results from 2-D computations and experimental observations. Our preliminary 3-D computations with a cylinder of $\mathrm{AR} = 5$ result in a mean lift coefficient of, approximately, 3·2. It is quite interesting to note that Prandtl observed a value of $C_L \sim 3{\cdot}2$ for a cylinder of $\mathrm{AR} = 4{\cdot}7$ and at $\mathrm{Re} = 5{\cdot}2 \times 10^4$ [as reported by Tokumaru & Dimotakis (1993) and Goldstein 1938]. However, on using end-plates of diameter 1·7 times the cylinder diameter, Prandtl observed that the value of the lift coefficient goes up to, approximately, 5. The results from the present 3-D computations correspond to the case without end-plates on the cylinder and the value of the lift coefficient

is quite close to that observed by Prandtl. The time histories for the lift and drag coefficient are shown in Figure 3. It can be observed that the 2- and 3-D time histories match quite well for some time, and later the 3-D effects become important and limit the value of lift coefficient that can be achieved. This observation is the same as the one that was made earlier in this section with respect to $\mathrm{Re} = 1000$ and $\alpha = 3$, that the discrepancy between the two-dimensional computational results and experimental results increases with time. These observations strengthen our proposition that it is the 3-D effects that play a key role in limiting the lift coefficient from a rotating cylinder and that the limit set by Prandtl's arguments may not hold. In fact, the data presented by Tokumaro & Dimotakis (1993) from their own experiments and that of others including Prandtl also suggests the same.

The set of results presented in this section demonstrate the ability of the present methodology in computing this class of flow problems quite effectively. It has also been shown that the flow past a rotating cylinder involves significant 3-D effects. However, in the rest of the article the computations with rotating control cylinders will be carried out in two-dimensions, with the understanding that the degree of control achieved in 2-D will set an upper bound for the control effectiveness that one should actually expect in real 3-D flows. The focus of the present paper is on flow control using rotating cylinders and the results in this section have been presented with a view to establish confidence in computing flows involving rotating cylinders. More results and details on the computation of flow past an isolated rotating cylinder will be presented in a later article.

4.2 Flow Past a Cylinder in the Presence of Two Control Cylinders

The diameter of the main cylinder is D while that of the control cylinder is D_2. All the results presented in this article are with $D/D_2 = 20$. The cylinders reside in a rectangular domain whose upstream and downstream boundaries are located at 8 and 30 cylinder diameters, respectively, from the centre of the main cylinder. The upper and lower boundaries are placed at 8 diameters each, from the centre of the main cylinder. The no-slip condition is specified for the velocity on the surface of the cylinders and free-stream values are assigned for the velocity at the upstream boundary. At the downstream boundary, we specify a Neumann-type boundary condition for the velocity that corresponds to zero viscous stress vector. On the upper and lower boundaries, the component of velocity normal to and the component of stress vector along these boundaries is prescribed zero value. The Reynolds number is based on the diameter of the main cylinder (D), free-stream velocity and the kinematic viscosity of the fluid.

The degree of flow control that can be achieved by utilizing rotating control cylinders depends on a variety of parameters. Some of them are the relative sizes of the main and control cylinders, their relative arrangements, and the rotation rates of the two control cylinders. Modi *et al.* (1991*a*, *b*, 1992) have reported results for flow control on bluff bodies for various rotation rates of the control cylinders. In the present article, in addition, the effect of the Reynolds number and the gap between the main and control cylinders is also investigated. Figure 4 shows the schematic of the typical arrangement of the set-up in the present work. Two control cylinders of diameter D_2, each, are placed close to the main cylinder such that the line joining the centres of the three cylinders is normal to the free-stream flow. The upper cylinder rotates in the clockwise and the lower one in the anticlockwise direction. The rotation rates of both the cylinders is Ω. In the rest of the article, the spin rates of the control cylinders will be expressed in terms of the ratio of the free-stream speed U and the tip speed of the rotating cylinders $U_c = D_2\Omega/2$. All the values for the lift and drag coefficients and the Strouhal number, reported in this article, have been

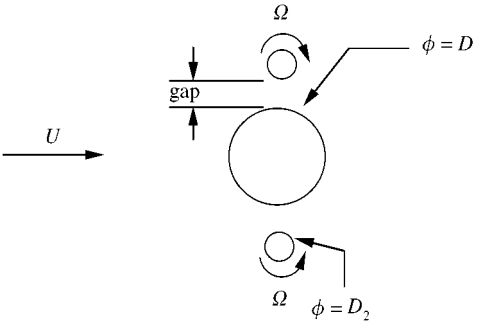

Figure 4. Description of the relative location of the main and control cylinders.

nondimensionalized with respect to the diameter of the main cylinder, D, and the free-stream speed, U. The quantities with suffix "1" refer to the main cylinder, while the ones with "2" and "3" correspond to the upper and lower control cylinders, respectively. It has been observed that the rotation of control cylinders at sufficiently high speed leads to a reduction in the drag coefficient for the main cylinder resulting in a saving of the power required for the translatory motion. However, the spinning of the control cylinders also requires a certain power input. In the present work, power coefficients for both translatory and rotational motion are computed. These coefficients are for the entire system. The power coefficient for translation includes the drag contribution from the main and the two control cylinders and that for the rotation is obtained from the torque (times angular velocity) required to rotate both the control cylinders. The power coefficient is nondimensionalized with the free-stream speed, dynamic pressure and diameter of the main cylinder. All the aerodynamic coefficients are reported per unit length of the main and control cylinders.

Computations are reported for two values of Reynolds number (Re = 100 and 10^4) and gap (= 0·01D and 0·075D). The rotating control cylinders generate circulation and inject momentum into the wake of the main cylinder. It is expected that if the gap between the main and control cylinders is too large, then, even though the control cylinders rotating at high speeds may generate enough circulation, their effect on the main cylinders will be small. On the other hand, if the gap is too small, the interaction between the main and control cylinders will be large, but the control cylinders will not be able to generate significant circulation to achieve good flow control. Therefore, the gap is an important parameter in obtaining the optimal performance of the flow control system.

A typical finite-element mesh and its close-ups, employed for the computation with gap = 0·01D, is shown in Figure 5. The flows that are being computed here involve the interaction of the wakes of the main and control cylinders. The disparity between the geometric scales of the main and control cylinders is expected to result in vortical structures of widely varying length scales, especially, for the Re = 10^4 flow. To resolve all the flow structures close to the cylinders, adequately, a structured finite-element mesh is used around the three cylinders. To minimize the grid size and to avoid the difficulties in generating a structured mesh around complex geometries (such as the gap), an unstructured mesh is generated using the Delaunay technique in the rest of the domain via an automatic mesh generator. All the finite-element implementations used for computations in this article are based on unstructured meshes and do not assume any structure of the mesh. The structured mesh close to the cylinders is utilized to have a control on the number of elements in the radial and circumferential directions.

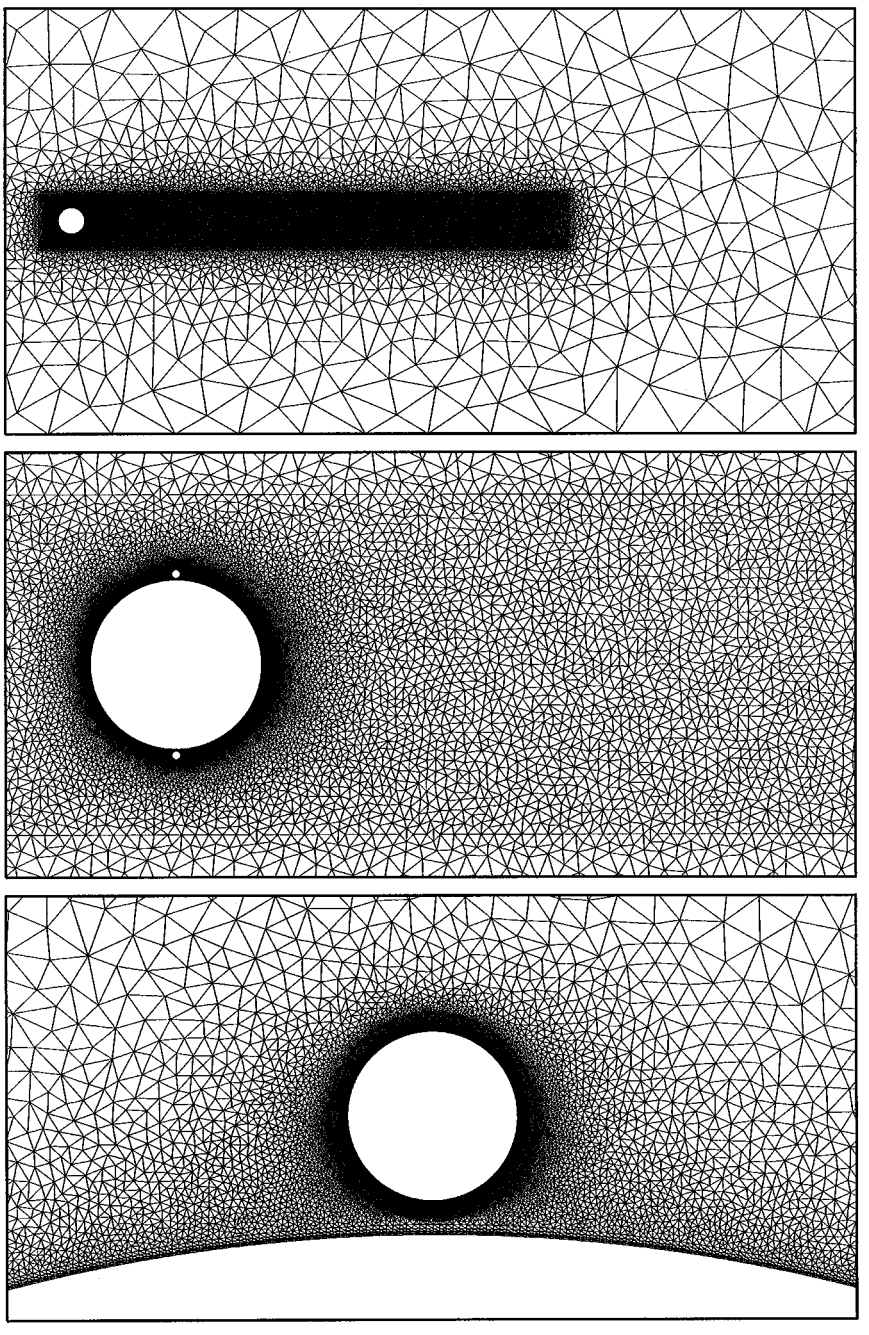

Figure 5. Flow past the main and control cylinders, gap = 0·01D: successive close-up views of the finite-element mesh with 55 228 nodes and 108 172 elements.

4.2.1. Re = 100, $D/D_2 = 20$, gap = 0·075D

The formulations and their implementations used in the present work are well proven and have been utilized to solve a variety of flow problems. Some applications can be found in the

articles by Mittal & Raghuvanshi (2000), Mittal *et al.* (1997) Tezduyar *et al.* (1992), Mittal (1992, 2000) and Behr *et al.* (1991, 1995). For example, they have been used to solve $\mathrm{Re} = 100$ flow past an isolated circular cylinder. This has now become a standard benchmark problem, and various researchers in the past have reported their computed results which are in good agreement with experimental observations. Behr *et al.* (1995) studied the effect of blockage caused by placing the lateral boundaries of the computational domain close to the cylinder. The investigation utilized two different formulations and led to the same conclusion. They found that if the lateral boundaries are brought too close to the cylinder, it results in a significant increase in the Strouhal number, amplitude of lift coefficient and mean drag coefficient. This has been kept in mind in deciding the location of the lateral boundaries in the present work. Mittal *et al.* and co-workers (1997, 2000) used formulations very similar to the one used in this article and reported results for Reynolds number between 60 and 1000. Their results are in excellent agreement with results from other researchers. For the flow at $\mathrm{Re} = 100$ they reported that the Strouhal number corresponding to the dominant frequency of the lift variation is 0·168, the mean drag coefficient is 1·402 and the amplitude of the lift coefficient is 0·355. Very recently, the same formulation as the one employed here, has been used by this author (Mittal 2000) to conduct a comprehensive study of the effect of the aspect-ratio of the elements in computing incompressible flows. $\mathrm{Re} = 100$ flow past a circular cylinder was used as one of the test cases. It was concluded that computations with grids that involve high aspect ratio triangular elements result in an unacceptable solution with some of the commonly used definitions of h (the element length). The best solution is provided by the definition of h that is related to the minimum edge-length of an element. The present computations have been carried out with the same definition of h.

Computations are initiated with the steady-state solution for the main and control cylinders at $\mathrm{Re} = 100$. Since an implicit time-integration scheme is being utilized to solve for the flow, a steady-state solution can be obtained by removing the unsteady terms from the governing equations. The steady-state solution is perturbed by rotating one of the control cylinders for a short time and again bringing it to rest. Our experience has shown that the fully developed time-periodic solution, for flow past an isolated cylinder, does not depend on the initial perturbations to the flow. Computation with an impulsive start for $U_c/U = 5$, presented later in the section, illustrates the same idea. Computations are carried with control cylinders at rest till the flow is fully developed and a temporally periodic solution is realized. At $t = 118{\cdot}5$ the upper control cylinder is assigned a clockwise rotation and the lower one an anticlockwise rotation such that the tip speed of the control cylinders is same as the free-stream speed of the flow, i.e., $U_c/U = 1$. The flow is allowed to develop, and at $t = 214{\cdot}6$ the rotational speed is doubled to give $U_c/U = 2$. Then, U_c/U is changed to 3, 4 and 5 at $t = 348{\cdot}2$, $440{\cdot}3$ and 704, respectively. Figure 6 shows the vorticity field for the fully developed flows at various rotation rates of the control cylinders. The flow patterns in the top row in this figure ($U_c/U = 0$) look very similar to that for a single isolated cylinder at the same Reynolds number. The Reynolds number based on the diameter of the control cylinder is 5. Therefore, no independent vortex-shedding is observed from the smaller cylinder. Vortex shedding takes place with the main and each control cylinder combined as a single body.

As the control cylinders start spinning and the rotation rate increases, the vortex-shedding frequency reduces and finally, at $U_c/U = 5$, the flow achieves a steady state. This is also accompanied by a narrowing of the wake. These observations are in concurrence with those made by Modi and his co-workers. Figure 7 shows the variation of the x component of fluid velocity in the gap region and close to the upper control cylinder for various rotation rates of the control cylinders. Shown in Figure 8 are the time histories of the lift and

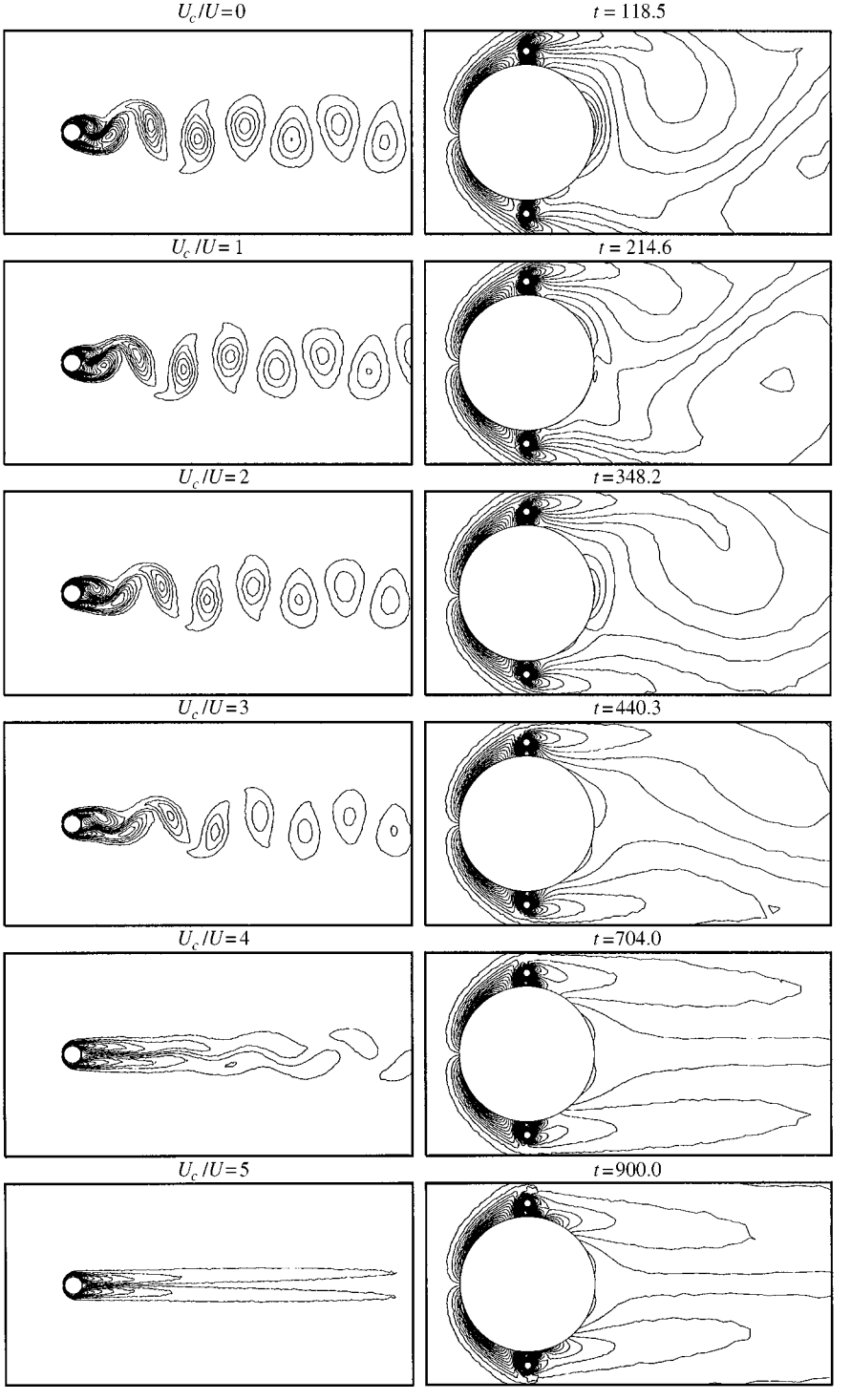

Figure 6. Re = 100 flow past main and control cylinders, gap = 0·075D: vorticity field and its close-up for the fully developed solution at various rotation rates of the control cylinders.

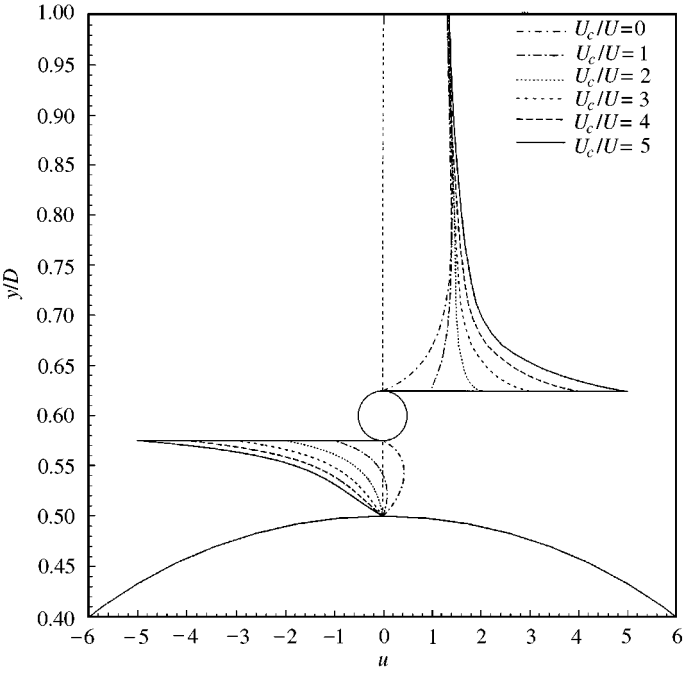

Figure 7. Re = 100 flow past main and control cylinders, gap = 0·075D: variation of the x component of velocity in the gap region and close to the upper control cylinder for various rotation rates.

drag coefficients of the three cylinders. For $U_c/U = 0$ the drag coefficient of the main cylinder (= 1·97) is higher than that experienced by an isolated cylinder. In addition, there is contribution to the total drag from the two control cylinders. Likewise, the amplitude of the lift coefficient experienced by the main cylinder (= 0·9) is significantly higher than that observed for an isolated cylinder. However, once the control cylinders start spinning, the drag and lift coefficients continue to drop as the rotation rate increases. For $U_c/U = 5$ the drag coefficient for the main cylinder is 0·73 and, since the flow achieves a steady state, the lift coefficient is zero. It is interesting to observe that under these conditions the control cylinders produce thrust. Of course, energy still needs to be put in to rotate them to overcome the aerodynamic moment. Recall, from the earlier section in this paper, the computations for an isolated rotating cylinders at $U_c/U = 5$ for Re = 5 result in a large value of the lift coefficient and a positive drag coefficient. One possible explanation for the negative drag coefficient observed in the present case is the following. The oncoming flow, according to an observer placed on the control cylinder, is at a slight angle to the free-stream flow due to the presence of the main cylinder. Therefore, the local lift vector is slightly tilted with respect to the free-stream direction and the effective drag coefficient (which is along the free-stream direction) gets a contribution from this tilted lift vector. For larger rotation rates, when the lift on the control cylinder is large, the drag component due to the tilt of the lift vector can become large thereby resulting in a negative drag coefficient.

Figure 9 shows the time histories of the power coefficient requirements (C_P) for the entire system for various rotation rates of the control cylinders. It is interesting to observe that the C_P required for translation keeps decreasing as the rotation rates of the control cylinders increase. However, the C_P required to rotate the control cylinders increases with the rotation speed. This suggests that there must be an optimal rotation rate at which the total

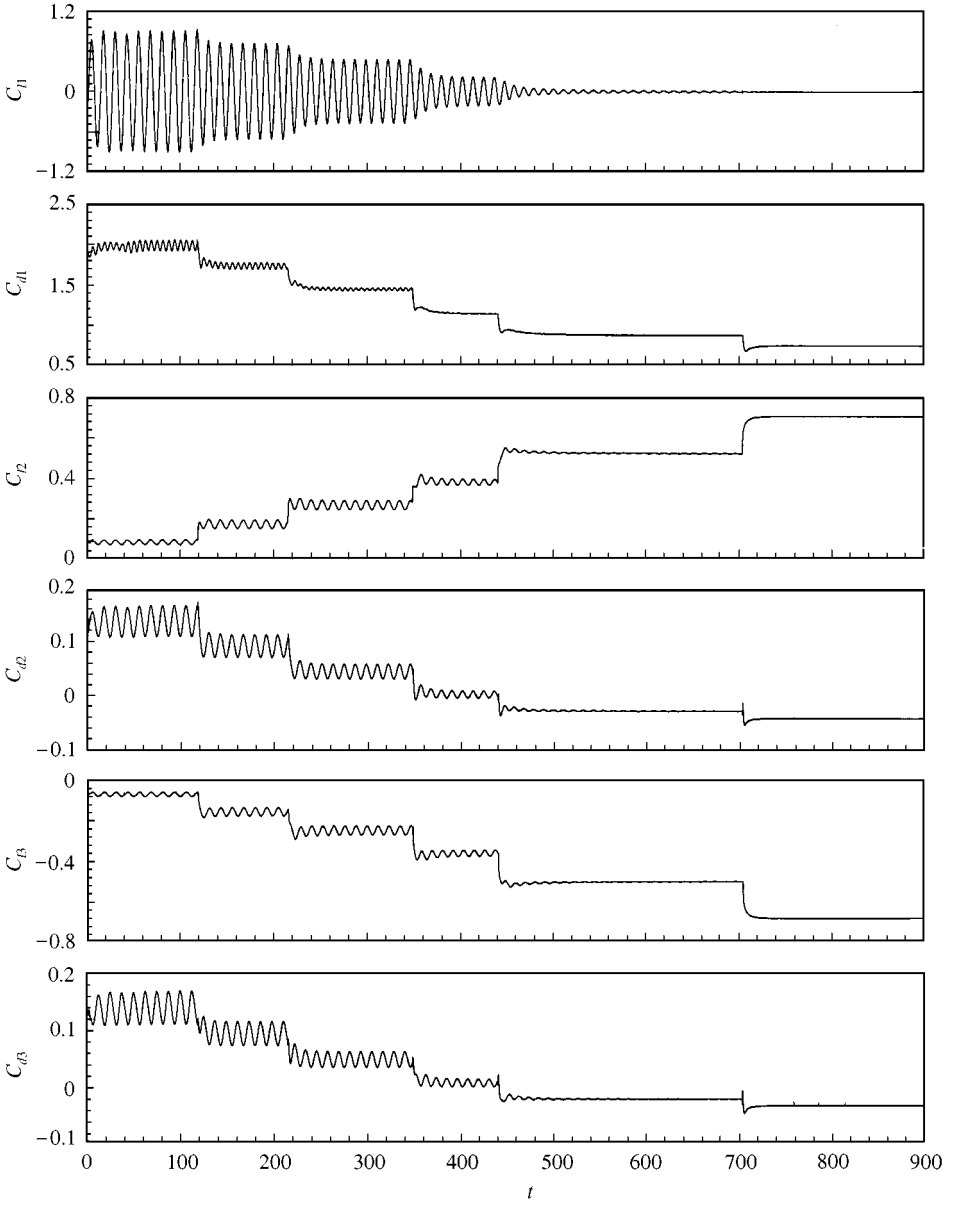

Figure 8. Re = 100 flow past main and control cylinders, gap = 0·075D, $U_c/U = \{0$ for $0 < t < 118{\cdot}5$, 1 for $118{\cdot}5 < t < 214{\cdot}6$, 2 for $214{\cdot}6 < t < 348{\cdot}2$, 3 for $348{\cdot}2 < t < 440{\cdot}3$, 4 for $440{\cdot}3 < t < 704$ and 5 for $t > 704\}$: time histories of the lift and drag coefficients. The upper two plots are for the main cylinder while the middle and lower two are for the upper and lower control cylinders, respectively.

power requirement of the system is minimum. The third panel in Figure 9 shows the time history of the total power requirement of the system for various rotation rates. It appears that $U_c/U = 5$ is very close to the optimal rotation rate with respect to the power requirement. Any further increase in the rotation rate will lead to an incremental reduction in drag coefficient but a significant increase in the power required to overcome the

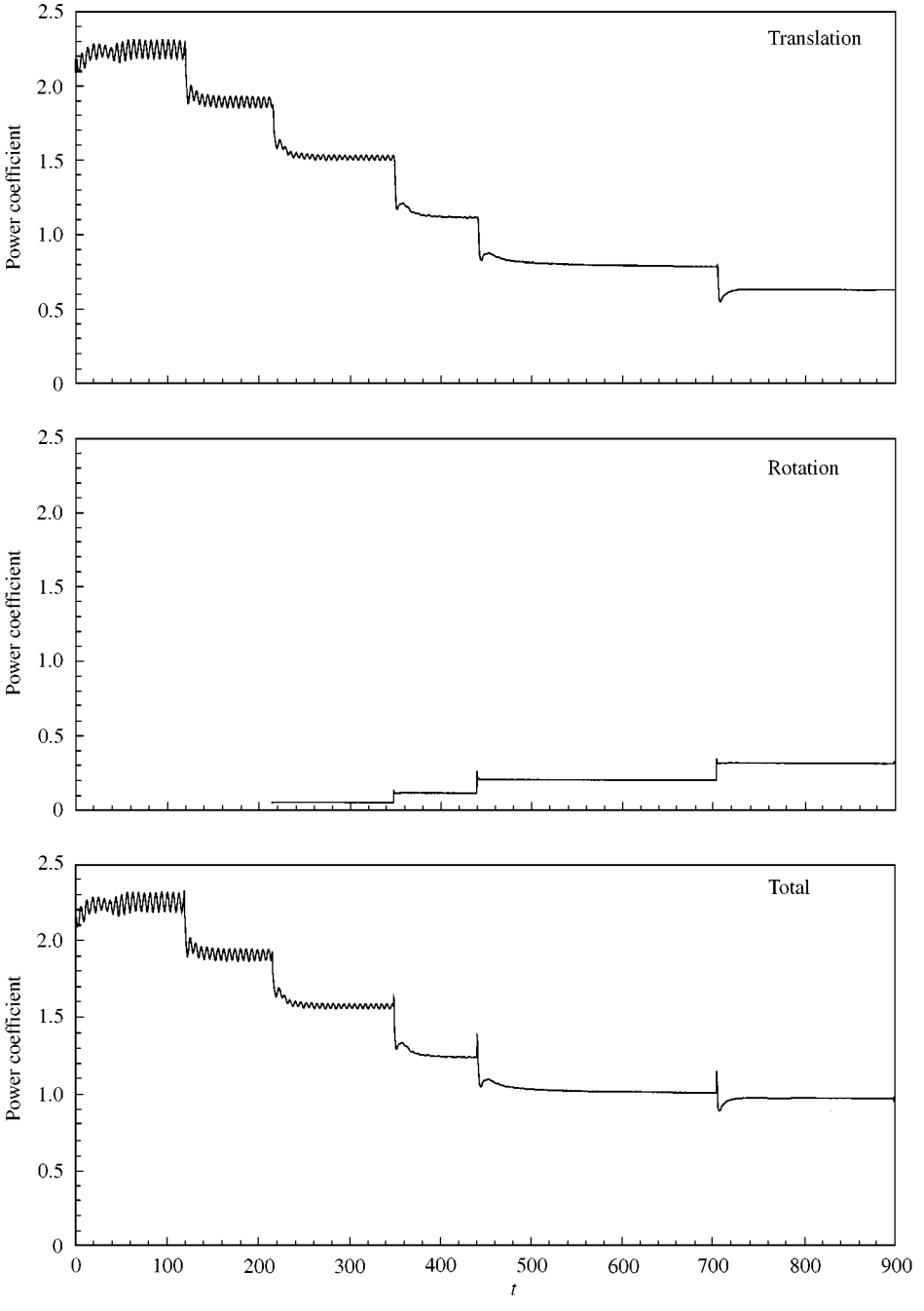

Figure 9. Re = 100 flow past main and control cylinders, gap = 0·075D, $U_c/U = \{0$ for $0 < t < 118{\cdot}5$, 1 for $118{\cdot}5 < t < 214{\cdot}6$, 2 for $214{\cdot}6 < t < 348{\cdot}2$, 3 for $348{\cdot}2 < t < 440{\cdot}3$, 4 for $440{\cdot}3 < t < 704$ and 5 for $t > 704\}$: time histories of the power coefficient.

rotational resistance, thereby leading to an increase in the overall power requirement. For an isolated cylinder, the power coefficient (required for its translational motion) is 1·4. For a cylinder, with control ($U_c/U = 5$), the total power coefficient is 0·97. That is a 40% saving on power if one excludes the frictional losses in the mechanisms of rotating cylinders. It is

interesting to note that, at Re = 100 and gap = 0·075D, approximately 33% of the total power is being used to overcome the resistance of the rotary motion of the control cylinders.

The set of computations that have been reported above have been carried out by scheduling the rotation of the control cylinders in a stepwise manner. To investigate the effect of specifying the rotation rate in steps of $U_c/U = 1$, we carry out another simulation that corresponds to an impulsive start. In this simulation, $U_c/U = 5$ is imposed on the surface of the control cylinders at $t = 0^+$. Eventually, the flow achieves a steady-state. It was observed, that the steady-state solution obtained from this simulation is exactly the same as the one obtained in the previous simulation with a different schedule of rotation of the control cylinders. The steady-state value of the aerodynamic coefficients in the two simulations is also the same. This reflects that the history of the rate of rotation of the control cylinders may not play an important role in deciding the final fully developed solution.

4.2.2. Re = 100, $D/D_2 = 20$, gap = $0.1D$

To study the effect of gap computations are carried out with a smaller gap between the main and control cylinders. The simulation begins with stationary control cylinders. U_c/U is changed to 1, 2 and 5 at $t = 52{\cdot}5$, 122·3 and 146·2, respectively. Figure 10 shows the vorticity field for the fully developed flows at various rotation rates of the control cylinders. As in the previous case, the flow for $U_c/U = 0$ looks very similar to that for a single cylinder at the same Reynolds number. For $U_c/U = 5$ the unsteadiness in the wake disappears and a steady-state solution is realized. Compared to the previous case, the smaller gap results in a significant effect of the main cylinder on the control cylinders. As can be noticed from the comparison of the pressure fields for the two cases for $U_c/U = 5$, the lower gap results in a upward movement of the saddle point for the rotating control cylinder. Figure 11 shows the variation of the x component of fluid velocity in the gap region and close to the upper control cylinder for various rotation rates of the control cylinders. For $U_c/U = 0$ the fluid remains stagnant in the gap region. Therefore, the flow upstream of the gap is forced to curve around the control cylinder. Compared to the large gap case, the width of the wake is smaller owing to a smaller frontal area. The narrower wake results in a lower value of the drag coefficient. Shown in Figure 12 are the time histories of the lift and drag coefficients of the three cylinders. For $U_c/U = 0$ the drag coefficient on the main cylinder (= 1.55) is lower than the large-gap case but still higher than that experienced by an isolated cylinder. For $U_c/U = 5$ the drag coefficient for the main cylinder reduces to 0·56. It can be observed that the lift generated by the control cylinders in the present case is smaller than that for the larger gap case. Since the lift is directly related to the circulation around the control cylinder, it may be concluded that the smaller gap results in a loss of circulation generation around the control cylinders. This observation is consistent with our earlier remarks regarding the flow pictures. Figure 13 shows the time histories of the power coefficient requirements for various rotation rates of the control cylinders. It is interesting to observe that for $U_c/U = 5$, compared to the large-gap case, the present case requires less power for translation but more for rotation. The overall power coefficient is 1·01 which is only about 4% higher than the large-gap case. It may, therefore, be concluded that for low Reynolds number flows the gap does not have a very significant effect on the overall power requirement of the system.

4.2.3. Re = 10^4, $D/D_2 = 20$, gap = $0.075D$

This value of Reynolds number is more realistic from the point of view of practical applications. Modi and his co-workers have conducted laboratory experiments related to

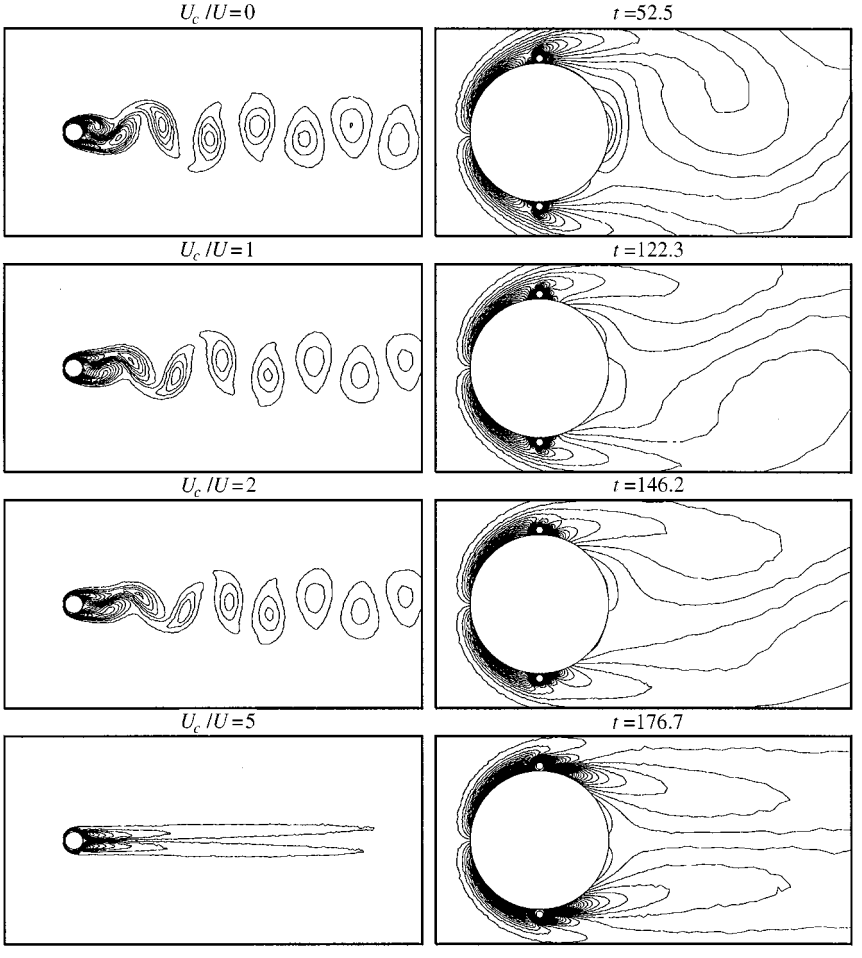

Figure 10. $Re = 100$ flow past main and control cylinders, gap $= 0{\cdot}01D$: vorticity field and its close-up for the fully developed solution at various rotation rates of the control cylinders.

this concept of flow control in the Reynolds number range of 3×10^4–10^5(Modi 1997). For the Re = 100 flow, the Reynolds number based on the control cylinder diameter is only 5. Therefore, no vortex shedding is seen from the control cylinder. In the present case, for the small cylinder Re = 500. Therefore, for stationary control cylinders and at low rotation rates the flow is expected to be extremely complex due to the interaction of the unsteady wake of the main and control cylinders. The finite-element mesh should be fine enough to resolve all the details of the complex flow. The computations begin with a mesh consisting of 22 221 nodes and 43 558 triangular elements and a time step of 0·02. In the structured part of the mesh around the main cylinder there are 600 elements in the circumferential and eight in the radial direction. The radial thickness of the band of structured elements is 0·025D. The band of elements around the control cylinders has a thickness of 0·0025D. It has 120 elements in the circumferential and four in the radial direction. The radial thickness of the elements close to the cylinders is $5 \times 10^{-4}D$. To check the effect of the time step and spatial resolution, the solution is projected on a finer mesh with 27 029 nodes and 53 014 elements and computations are continued with a reduced time step of 0·01. The mesh with larger

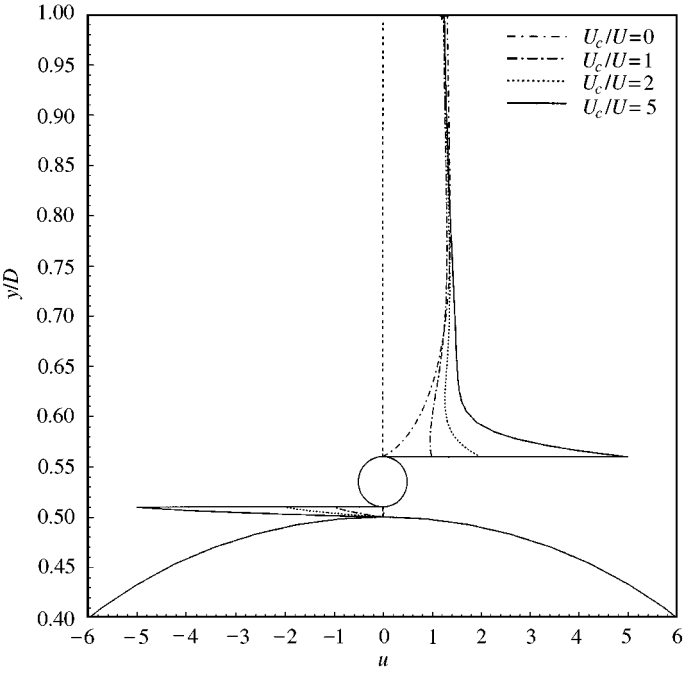

Figure 11. Re = 100 flow past main and control cylinders, gap = 0·01D: variation of the x component of velocity in the gap region and close to the upper control cylinder for various rotation rates.

number of nodes is similar to the other one except for more refinement close to the control cylinders and the gap. In the regions close to the control cylinder it is, approximately, twice as refined as the earlier one. This mesh has 200 elements in the circumferential and eight in the radial direction in the annulus consisting of the structured part of the mesh around the control cylinders. The first element thickness, in this case, is $5 \times 10^{-5}D$. The solutions computed on the two meshes do not show any appreciable difference except for a slight increase (less than 2%) in the amplitude of the unsteady aerodynamic coefficients with the refined mesh. The rest of the computations have been carried out with the refined mesh and a time step of 0·01. U_c/U is changed to 5 and 6 at t = 129·55, and 212·49, respectively. The time step for the cases with rotating control cylinders is 0·001.

Figure 14 shows the vorticity and pressure fields for the fully developed flows at various rotation rates of the control cylinders. The top two rows in this figure are for $U_c/U = 0$. The wake appears quite disorganized compared to that observed at lower Reynolds number. The global view of the flow field looks quite similar to that for an isolated single cylinder at the same Reynolds number as shown by Mittal & Kumar (2000). A close-up view, however, shows the intricate interactions between the unsteady wakes of the control and main cylinder. As expected, both the control cylinders are associated with a vortex street, each. The finite-element mesh does a good job in resolving the vortices shed from the control cylinders that are of a much smaller length scale, compared to the main cylinder diameter. Within a very short distance downstream of the cylinders, the vortices shed from the control cylinders are dissipated. For $U_c/U = 5$ the wake reorganizes itself. It is much narrower and the flow achieves a temporally periodic state. Recall that the Re = 100 flow for the same arrangement of control cylinders results in a steady flow for $U_c/U = 5$. This points to a strong Reynolds number dependence of the flow, at least in this range. From the

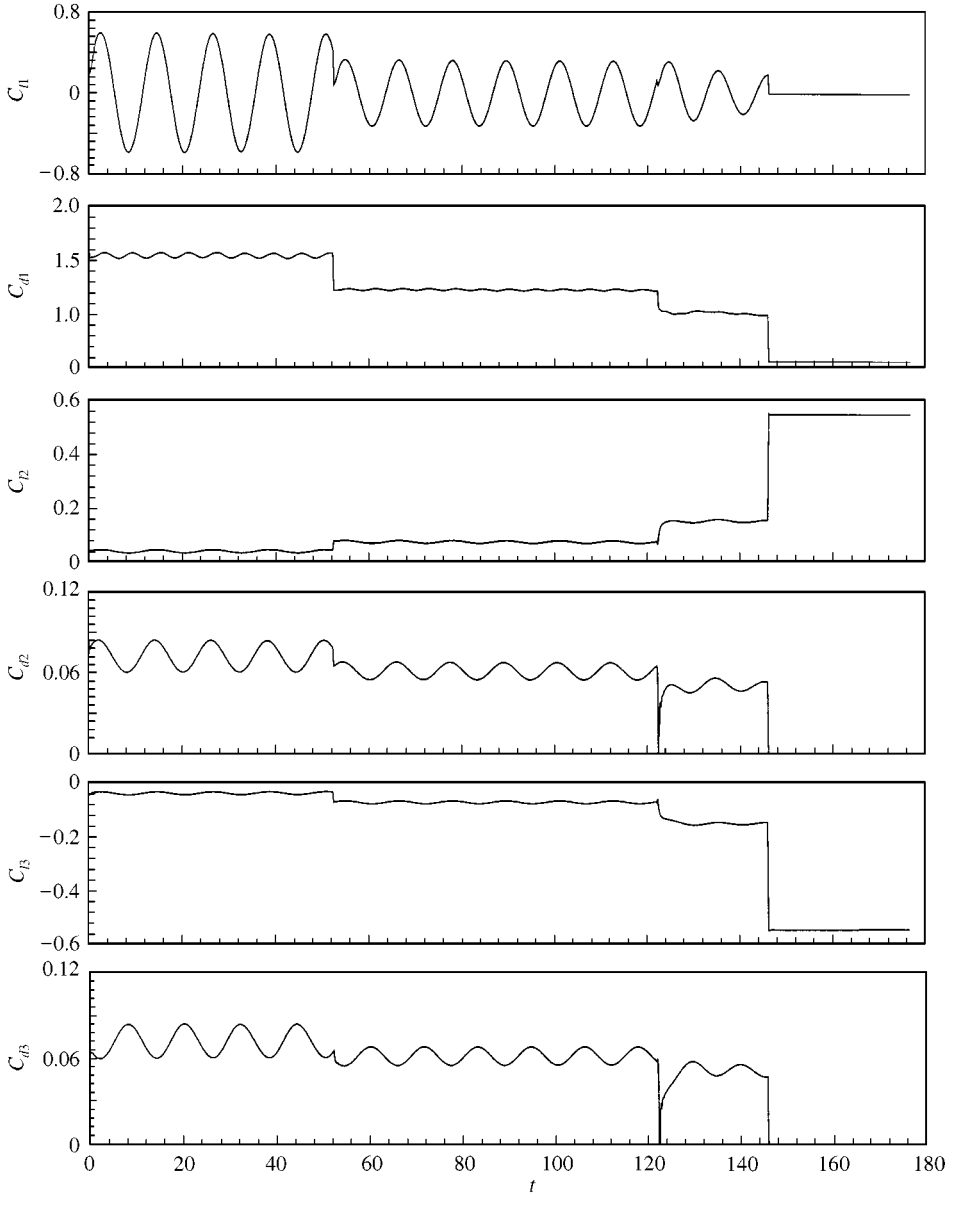

Figure 12. Re = 100 flow past main and control cylinders, gap = 0·01D, $U_c/U = \{0$ for $0 < t < 52{\cdot}5$, 1 for $52{\cdot}5 < t < 122{\cdot}3$, 2 for $122{\cdot}3 < t < 146{\cdot}2$ and 5 for $t > 146{\cdot}2\}$: time histories of the lift and drag coefficients. The upper two plots are for the main cylinder while the middle and lower two are for the upper and lower control cylinders, respectively.

comparison of the close-up views of the cases for $U_c/U = 0$ and 5 it can be observed that the high-speed rotation of the control cylinders leads to a reattachment of the flow on the leeward side of the main cylinder resulting in a delay of separation and a much narrower wake. Also, the vortex shedding that is observed for the stationary control cylinders ceases to take place for $U_c/U = 5$. The qualitative behaviour of the flow for $U_c/U = 6$ remains the same as for $U_c/U = 5$.

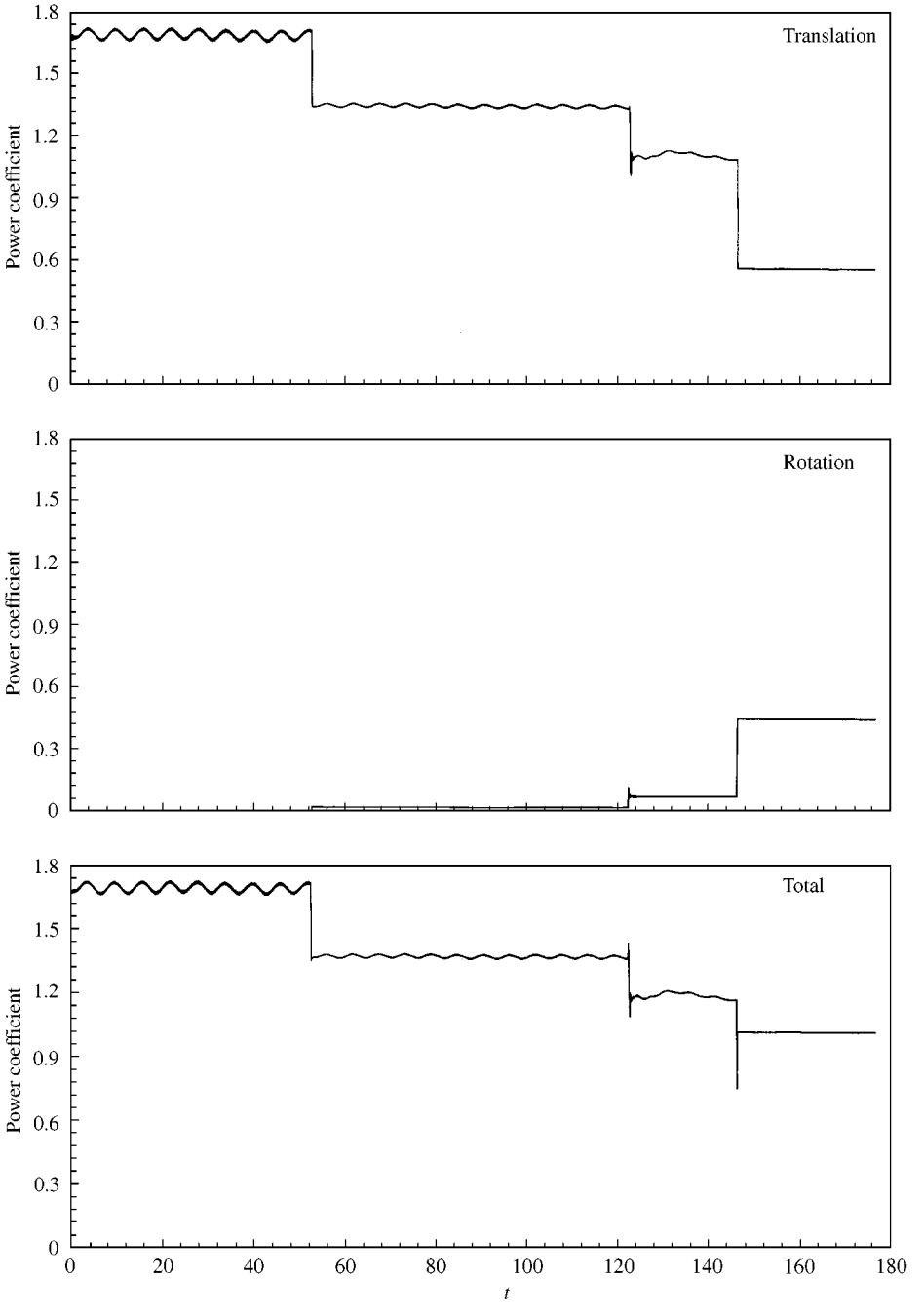

Figure 13. Re = 100 flow past main and control cylinders, gap = 0·01D, $U_c/U = \{0$ for $0 < t < 52{\cdot}5$, 1 for $52{\cdot}5 < t < 122{\cdot}3$, 2 for $122{\cdot}3 < t < 146{\cdot}2$ and 5 for $t > 146{\cdot}2\}$: time histories of the power coefficient.

Figure 15 shows the variation of the x component of fluid velocity in the gap region and close to the upper control cylinder for various rotation rates of the control cylinders. It is interesting to compare this figure with that for the Re = 100 flow (Figure 7). For the

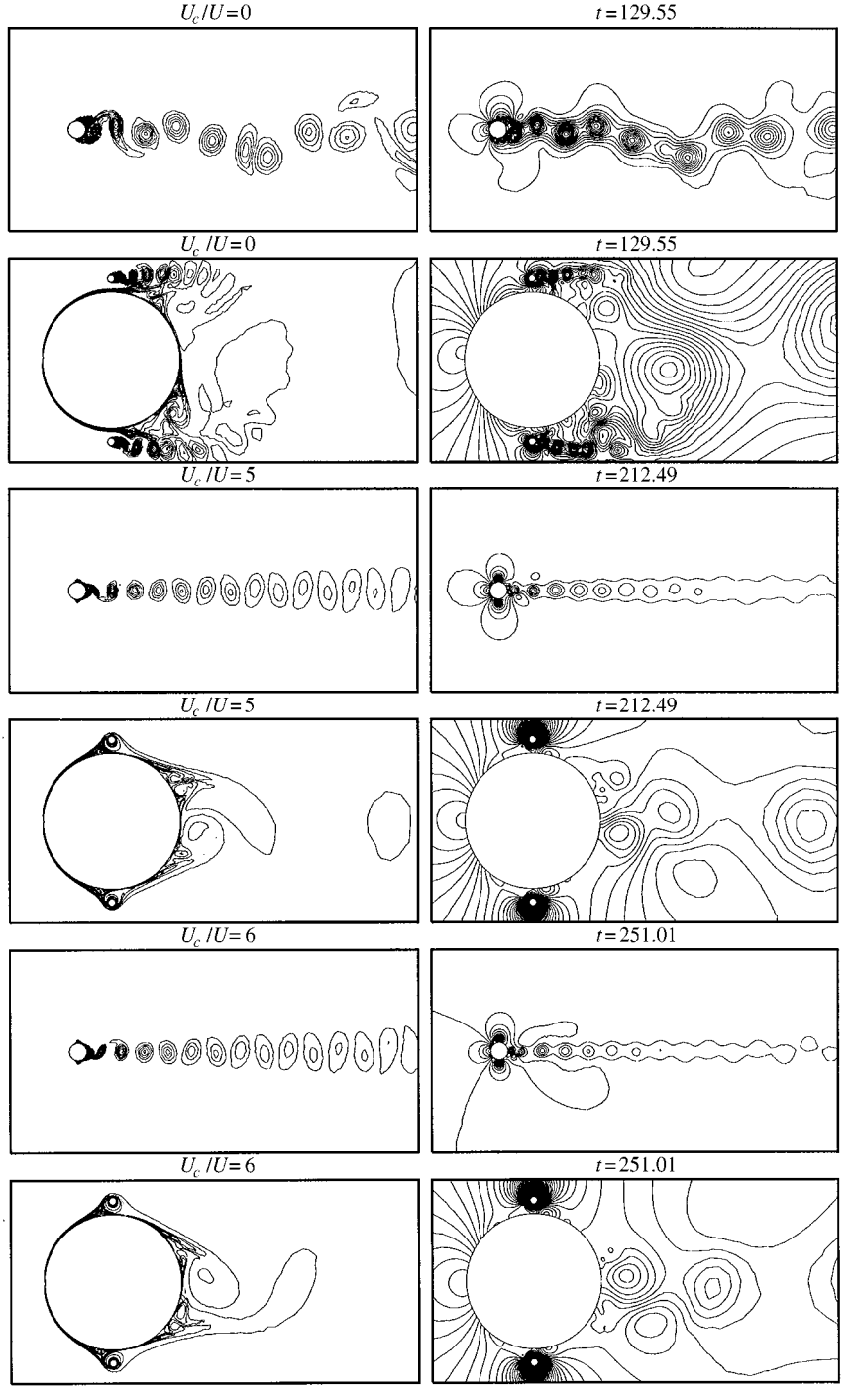

Figure 14. $\mathrm{Re} = 10^4$ flow past main and control cylinders, gap $= 0{\cdot}075D$: vorticity (left) and pressure (right) fields and their close-ups for various rotation rates of the control cylinders.

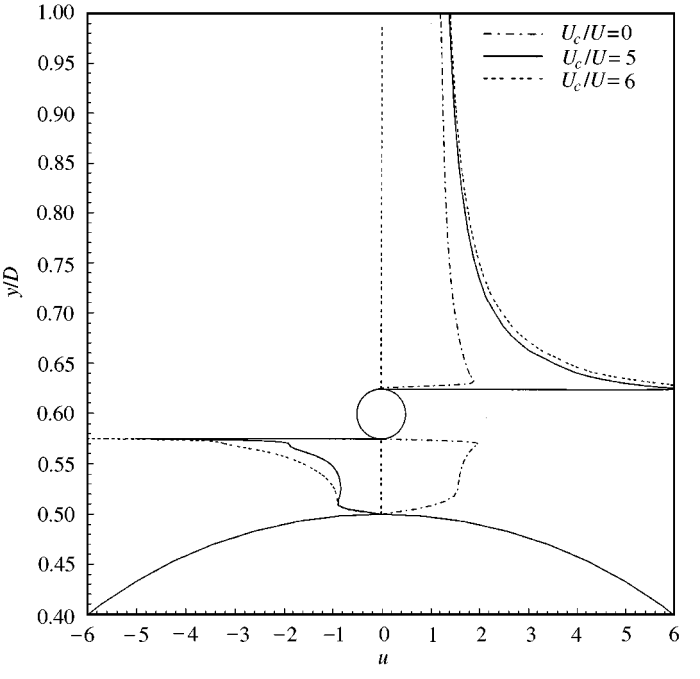

Figure 15. Re = 10^4 flow past main and control cylinders, gap = 0·075D: variation of the x component of velocity in the gap region and close to the upper control cylinder for various rotation rates.

Re = 100 case the velocity profile in the gap is almost parabolic with a peak speed that is, approximately, half of the free-stream speed. The shear stresses acting on the main and control cylinders in the gap region are comparable. For the Re = 10^4 case, the boundary layers on the main and control cylinders in the gap region are quite thin and the shear stress acting on the control cylinder is larger than that on the main cylinder. When the control cylinders are rotating, the velocity profile in the gap region of the Re = 10^4 flow shows inflection points which are absent in the Re = 100 flow. Also, the effect of the rotation persists to a larger distance above the control cylinder for the Re = 10^4 flow than for the Re = 100 case.

Shown in Figure 16 are the time histories of the lift and drag coefficients for the three cylinders. For $U_c/U = 0$ it can be observed that the drag and lift signature of the control cylinders is associated with two frequencies that correspond to the vortex shedding frequencies of the main and control cylinders. The main cylinder also feels the unsteadiness caused by the vortex shedding from the control cylinders and it appears as a high-frequency variation in the time histories for its aerodynamic coefficients. The mean drag coefficient for the main cylinder is 1·6, approximately. This value is slightly higher than that observed for a single isolated cylinder ($\approx$ 1·5) at Re = 10^4 as reported by Mittal & Kumar (2000). As expected, because of the presence of the main cylinder, the mean lift coefficient for the upper control cylinder is slightly positive and that for the lower one slightly negative. The rotation of the control cylinders lead to a reduction in the drag acting on the system. The mean drag coefficient for the main cylinder for $U_c/U = 5$ is 0·47. A further increase in U_c/U to six causes only a marginal reduction in the mean drag coefficient. The mean lift coefficient for the present case is significantly larger than that seen for the Re = 100 flow, again suggesting a strong Reynolds number effect in this range of Re.

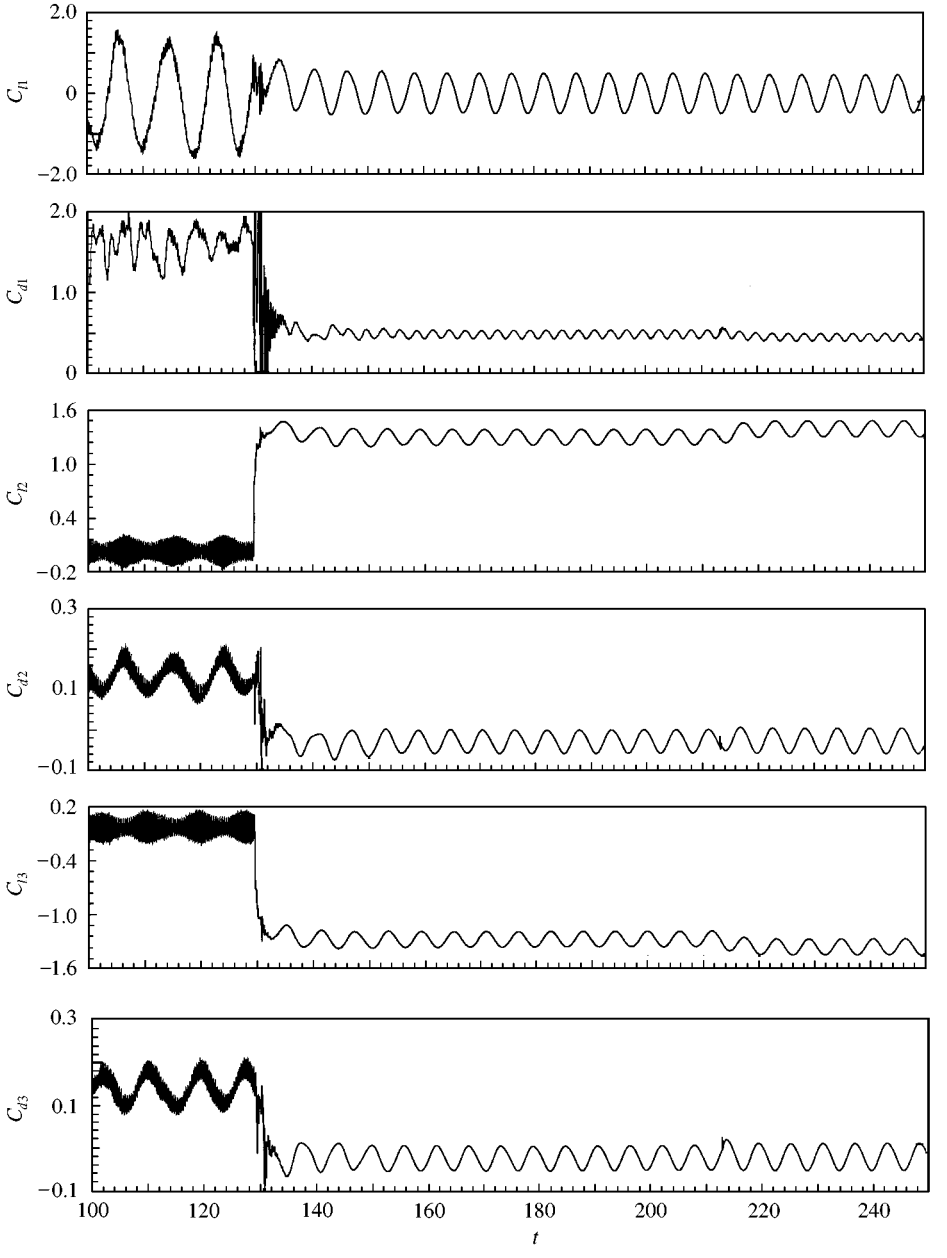

Figure 16. $\mathrm{Re} = 10^4$ flow past main and control cylinders, gap $= 0{\cdot}075D$, $U_c/U = \{0$ for $0 < t < 129{\cdot}55$, 5 for $129{\cdot}55 < t < 212{\cdot}49$, and 6 for $t > 212{\cdot}49\}$: time histories of the lift and drag coefficients. The upper two plots are for the main cylinder while the middle and lower two are for the upper and lower control cylinders, respectively.

An interesting observation as a result of this computation comes from Figure 17 that shows the time histories of the power coefficient requirements for various rotation rates of the control cylinders. Unlike the $\mathrm{Re} = 100$ case, the power coefficient required to rotate the control cylinders at high Reynolds number is negligible. Consequently, the total mean power coefficient required for the system is much lower for $\mathrm{Re} = 10^4$ ($= 0{\cdot}41$) as compared

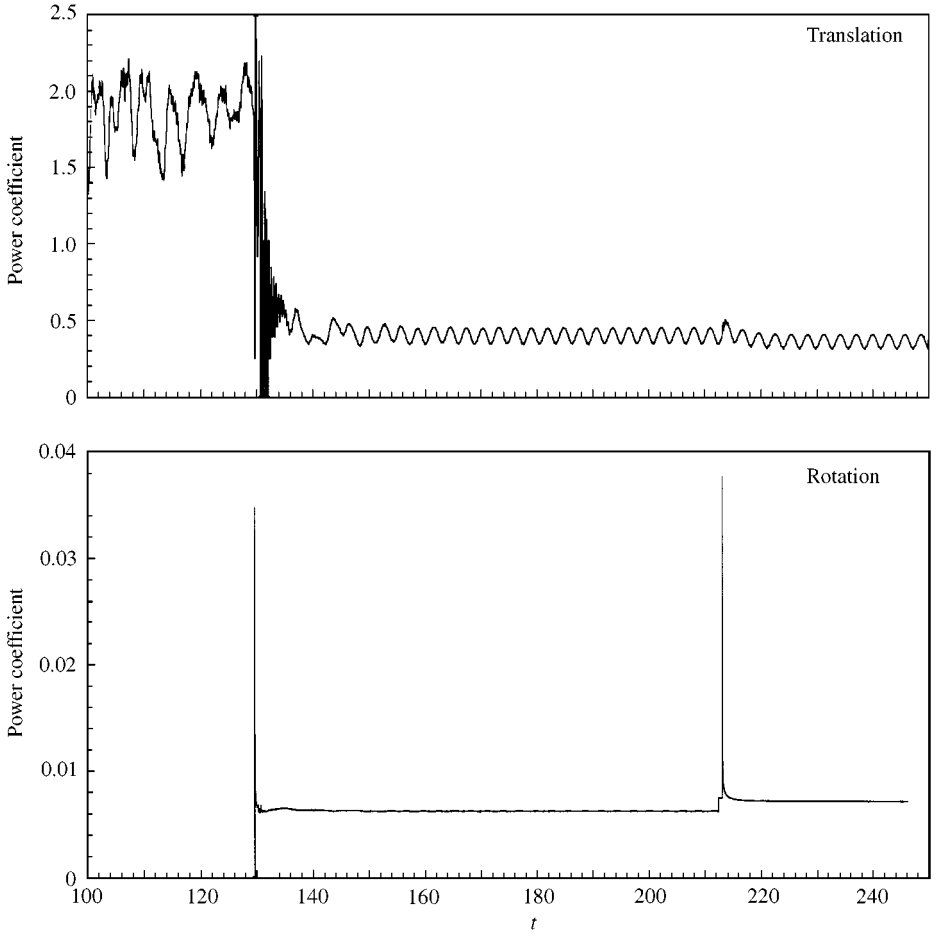

Figure 17. $\mathrm{Re} = 10^4$ flow past main and control cylinders, gap $= 0{\cdot}075D$, $U_c/U = \{0$ for $0 < t < 129{\cdot}55$, 5 for $129{\cdot}55 < t < 212{\cdot}49$, and 6 for $t > 212{\cdot}49\}$: time histories of the power coefficient.

to the $\mathrm{Re} = 100$ flow ($= 0{\cdot}97$). Compared to a single cylinder at $\mathrm{Re} = 10^4$, the flow control with $U_c/U = 5$ results in a 78% saving in power. Of course, this does not include the mechanical losses in various components of the system. In addition to a reduction in drag coefficient there is also a significant reduction in the unsteady forces acting on the body that reduces the flow-induced vibrations.

4.2.4. $\mathrm{Re} = 10^4$, $D/D_2 = 20$, gap $= 0{\cdot}01D$

In this section, results are presented for the $\mathrm{Re} = 10^4$ flow and smaller gap. Figure 18 shows the vorticity and pressure fields for the fully developed flows at various rotation rates of the control cylinders. The top two rows in this figure are for $U_c/U = 0$. The wake in the present case looks quite different from the one with gap $= 0{\cdot}075D$. It is much wider and is associated with the pairing of vortices. The vortex shedding from the control cylinders is intermittent. Vortices are shed from both the upper and lower surfaces of the control cylinders. However, because of the small gap between the main and control cylinders, the vortex shed from the surface facing the gap is weaker than the other one. Unlike the earlier simulations, the

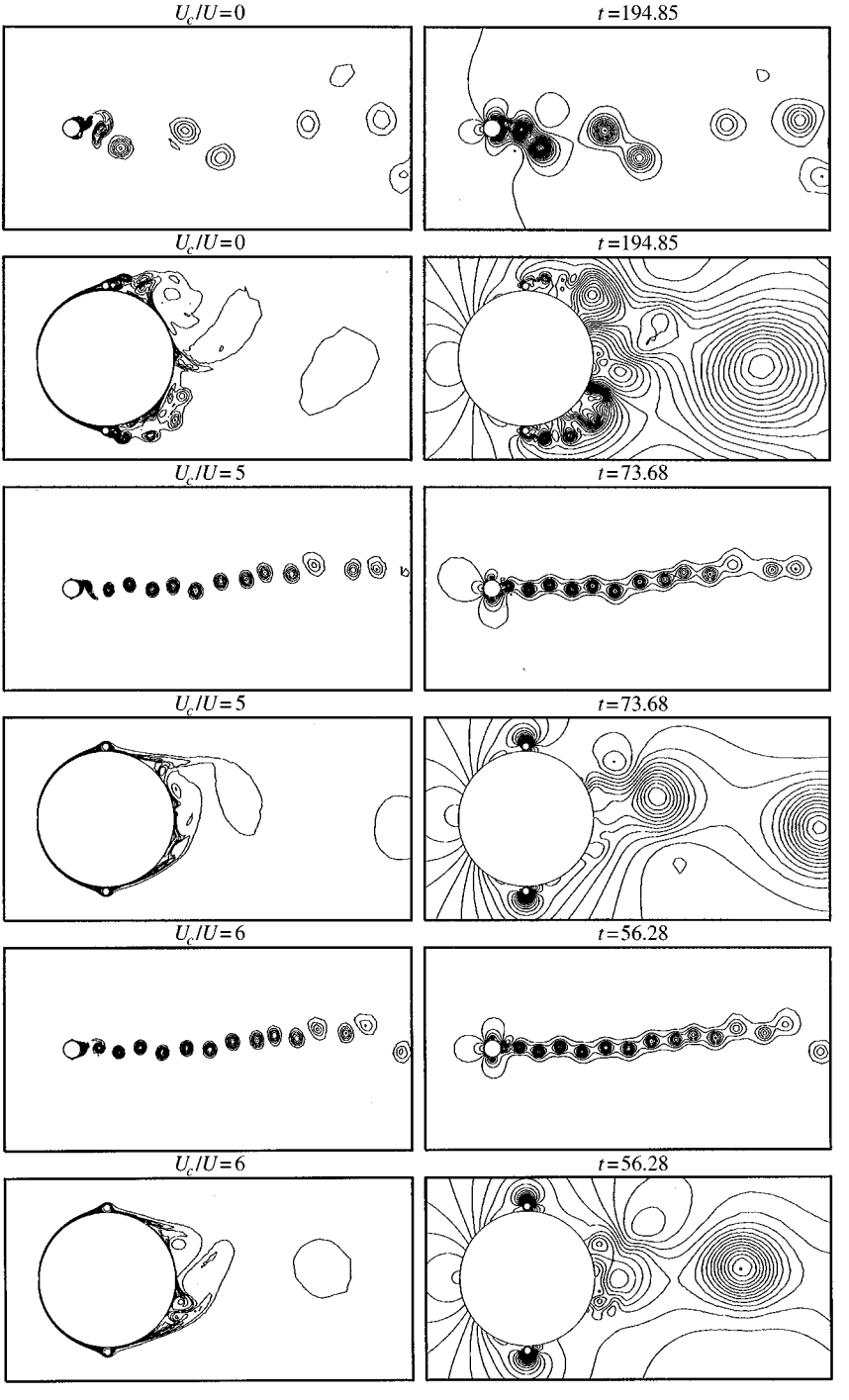

Figure 18. Re $= 10^4$ flow past main and control cylinders, gap $= 0{\cdot}01D$: vorticity (left) and pressure (right) fields and their close-ups for various rotation rates of the control cylinders.

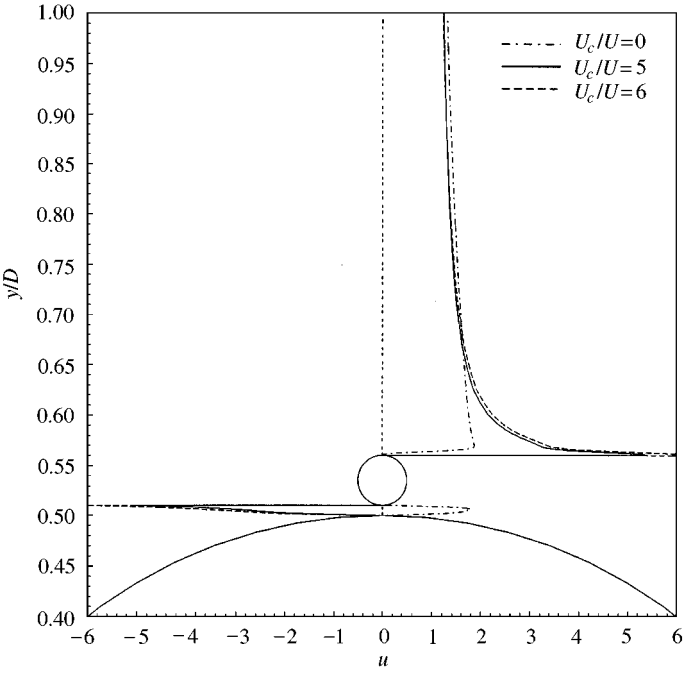

Figure 19. $\mathrm{Re} = 10^4$ flow past main and control cylinders, gap $= 0{\cdot}01D$: variation of the x component of velocity in the gap region and close to the upper control cylinder for various rotation rates.

rotation rate of the control cylinders is not stepped up during the simulation. The computations are initiated from steady-state solutions at $\mathrm{Re} = 100$. As in the earlier cases, the rotation of the control surfaces lead to organization of the wake and its narrowing. The vortex shedding from the control cylinders also ceases as a result of the rotation. Compared to the large-gap case, the wake in the present case seems to have a bias towards the upper half plane with respect to the streamwise direction. Such a bias is also observed for flow past isolated cylinders at moderate Reynolds number and is perhaps caused by interaction between strong vortices. This has also been reported by Behr (1992). Figure 19 shows the variation of the x component of fluid velocity in the gap region and close to the upper control cylinder for various rotation rates of the control cylinders. Unlike the $\mathrm{Re} = 100$ case the velocity profile for $U_c/U = 0$ suggests the presence of *a jet* in the gap between the main and control cylinders. The centreline velocity of the gap flow is almost twice that of the free-stream velocity.

Shown in Figure 20 are the time histories of the lift and drag coefficients of the three cylinders. For $U_c/U = 0$ this picture shows intermittent vortex shedding from the two control cylinders. For $U_c/U = 5$ and above, vortex shedding for the control cylinders disappears and a reduction in the drag coefficient for the main cylinder is observed. Compared to the large gap case, the drag reduction in the present case is much smaller. The mean lift coefficient in the present case experienced by the control cylinders is much smaller than that in the previous case suggesting a lower circulation in the present case. Figure 21 shows the time histories of the power coefficient requirements for various rotation rates of the control cylinders. Again, the power required for the rotation of the control cylinders is extremely small. However, the saving in the power required for translation of the system due to flow control is not as spectacular as observed in the previous case. This suggests that the

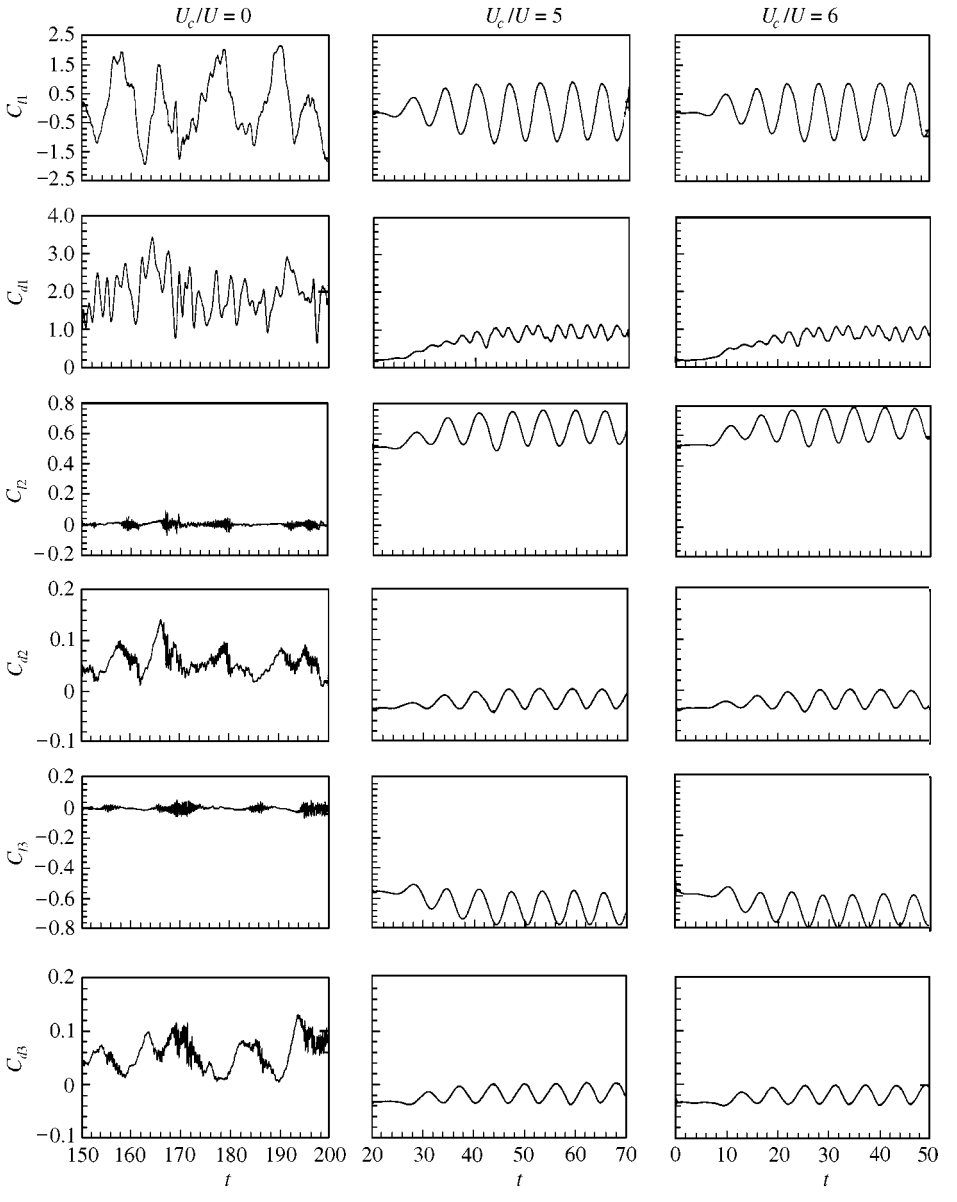

Figure 20. Re = 10^4 flow past main and control cylinders, gap = 0·01D, $U_c/U = 0$, 5 and 6: time histories of the lift and drag coefficients. The upper two rows of plots are for the main cylinder while the middle and lower two are for the upper and lower control cylinders, respectively.

gap plays an important role in such flows that involve rotating control cylinders, and more work needs to be done to estimate the optimal gap.

Shown in Figure 22 is the variation of the pressure coefficient (C_p) along the surface of the main and control cylinders for various values of the gap and Re for $U_c/U = 5$. The C_p plots for the main cylinder for the Re = 100 flow indicate the same value of the pressure on the upper and lower surfaces of the cylinder for both the big and small gap. This is consistent with the observation that the lift coefficient in both the cases is zero. For the Re = 10^4 flow the C_p values on the upper and lower surfaces are different, indicating a net lift force acting

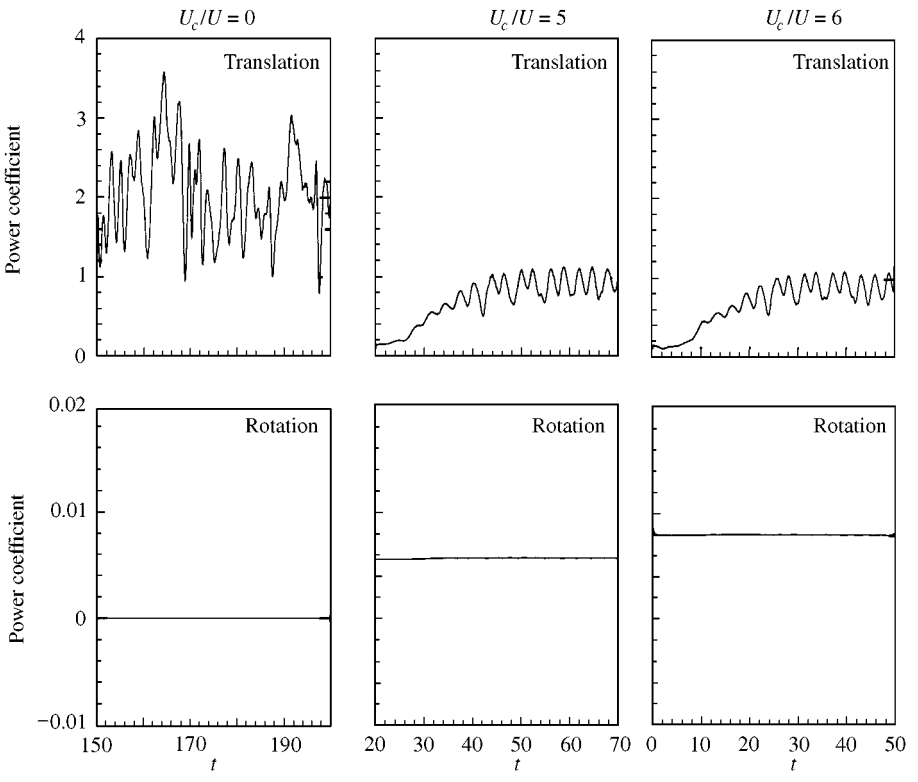

Figure 21. Re = 10^4 flow past main and control cylinders, gap = 0.01D, $U_c/U = 0$, 5 and 6: time histories of the power coefficient.

on the main cylinder. The departure from symmetry of the C_p plot about a vertical line passing through the centre of the cylinder is an indicator of the drag acting on it. This observation can be used to explain the cause of generation of thrust from control cylinders in some cases. The high value of $-C_p$ on the control cylinders, especially, at Re = 10^4 indicates the high level of circulation generated because of the high spin rates. The C_p plots for the Re = 100 and gap = 0·01D stand out from the rest. The rotation of the cylinders causes the surrounding fluid to be dragged along with them. If the gap between the main and rotating control cylinders is too small, not all the fluid can pass through the gap, and a part of this high-speed moving fluid impinges on the main cylinder slightly downstream of the gap, leading to a very high stagnation pressure. With an increase in Reynolds number, the mass of fluid dragged with the rotating cylinder decreases. A much milder version of the same phenomenon is observed for the Re = 10^4 flow.

5. CONCLUDING REMARKS

Control of flow past a circular cylinder, using rotating cylinder elements, has been studied numerically. A stabilized finite-element method is utilized to solve the incompressible Navier–Stokes equations in the primitive variables formulation. First, the formulation is utilized to study the flow past an isolated rotating cylinder. Excellent agreement with some of the flow visualizations carried out by other researchers, earlier, is observed. At high rotation rates it is seen that the lift for purely two-dimensional set-up can be very large. The

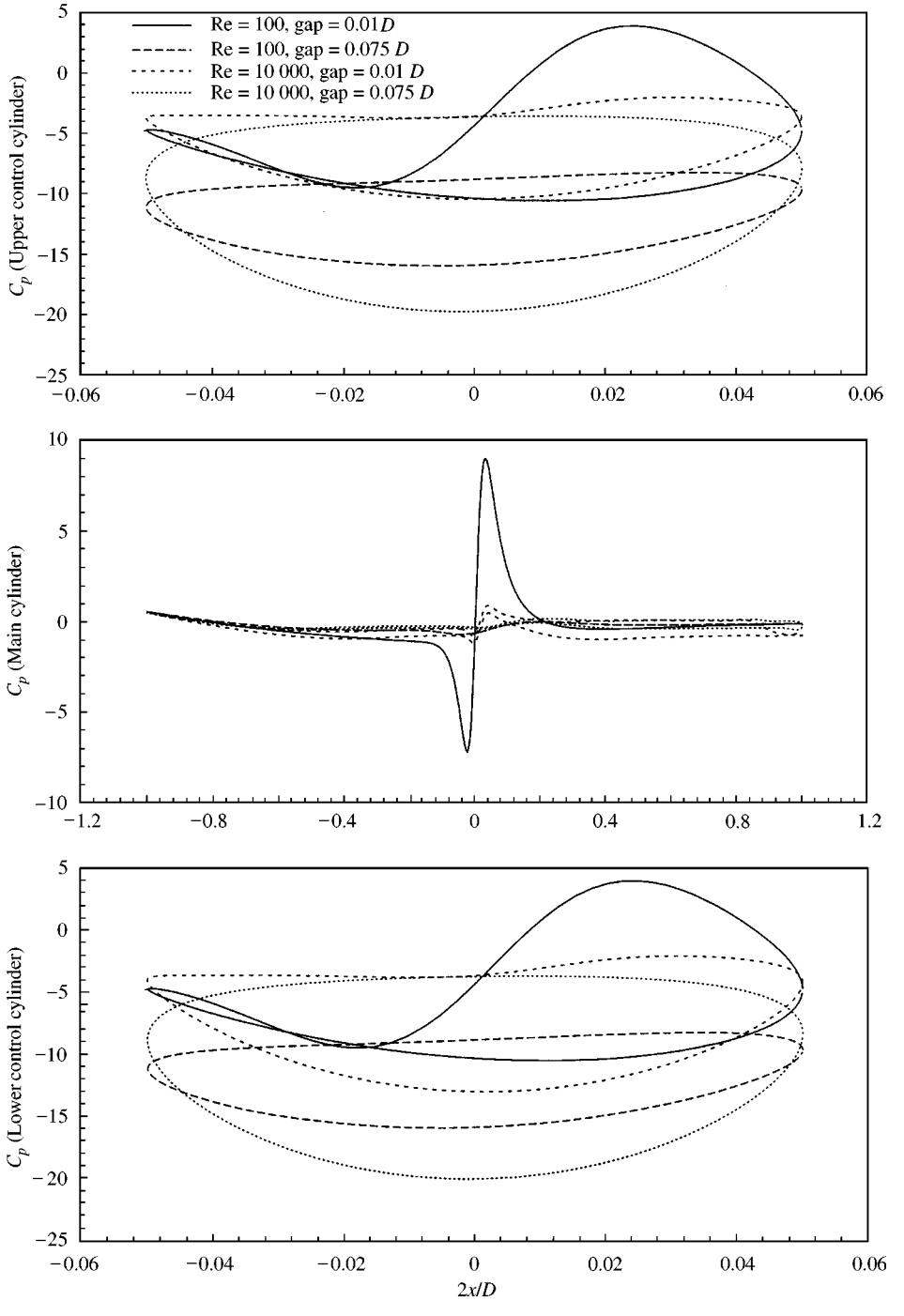

Figure 22. Flow past main and control cylinders, $U_c/U = 5$: variation of the pressure coefficient along the surface of the main and control cylinders for various values of gap and Reynolds number.

TABLE 1
Flow past main and control cylinders with $U_c/U = 5$: summary of the coefficient of power required for rotation and translation

Re	Gap	$C_{\text{power}}^{\text{rot}}$	$C_{\text{power}}^{\text{transl}}$	$C_{\text{power}}^{\text{total}}$
100	0·010 D	0·45	0·56	1·01
100	0·075 D	0·32	0·65	0·97
10 000	0·010 D	0·006	0·95	0·96
10 000	0·075 D	0·006	0·40	0·41

values of the lift coefficient obtained in the present work exceed the maximum limit based on the arguments of Prandtl. It is also found, via computations in 3-D, that the aspect ratio of the cylinder (spanwise length/diameter) is an important parameter for the amount of lift generated by the rotating cylinder. The end-effects cause separation of flow and the entire span is infected with centrifugal instabilities. Both these effects contribute to the loss of lift compared to that seen for a purely two-dimensional case. Good comparison between the 3-D computational results and the experimental results for mean value of lift coefficient is seen. These simulations increase our confidence in the present formulations and their implementations. In addition they contribute to our understanding of the flow past a spinning and translating cylinder that form the heart of the present flow control mechanism.

Simulations are carried out for two values of the Reynolds number ($\text{Re} = 10^2$ and 10^4) and gap between the main and control cylinders (gap $= 0{\cdot}01D$ and $0{\cdot}075D$). The results are in good agreement with the flow-visualization studies conducted by other researchers for bluff bodies using similar control concepts. It is observed that $U_c/U = 5$ results in a steady flow at low Reynolds numbers. At $\text{Re} = 10^4$, even though the flow remains unsteady, the wake is highly organized and narrower compared to the one without control. In all the cases, a significant reduction in the overall drag coefficient and the unsteady aerodynamic forces acting on the body is observed. The reduction in unsteady forces leads to an alleviation of the flow-induced vibrations of the body. The effect of the gap is found to be more critical for the $\text{Re} = 10^4$ flows compared to that at lower Reynolds numbers. Another interesting observation from this study is regarding the effect of Reynolds number on the power required to rotate the control cylinders to overcome the aerodynamic resistance. It is found that the coefficient of power required for rotating the control cylinders is significant for low but negligible for relatively higher Reynolds number (10^4) flows. A summary of the power requirements for the various cases is given in Table 1.

This study brings out the Reynolds number effect in such flows and the relevance of the gap as a design parameter for such flow control devices. An effort to investigate the effect of the gap in detail is underway. The circulation generated by the rotating control cylinders is an important component of this flow control mechanism and its sensitivity to three-dimensional effects has already been demonstrated. The extension of this effect to flow control using rotating cylinders is another area that needs to be studied. The 2-D computations set an upper bound on the control effectiveness of the rotating cylinders, and it is expected that actual behaviour of such control strategies depend significantly on three-dimensional effects.

ACKNOWLEDGEMENT

Partial support for this work has come from the Department of Science and Technology, India, under project number DST-AE-95279 with the Department of Aerospace Engineering, IIT, Kanpur.

References

Badr, H. M., Coutanceau, M., Dennis, S. C. R. & Menard, C. 1990 Unsteady flow past a rotating cylinder at Reynolds numbers 10^3 and 10^4. *Journal of Fluid Mechanics* **220,** 459–484.

Badr, H. M. & Dennis, S. C. R. 1985 Time-dependent viscous flow past an impulsively started rotating and translating circular cylinder. *Journal of Fluid Mechanics* **158,** 447–488.

Behr, M. 1992 Stabilized finite element methods for incompressible flows with emphasis on moving boundaries and interfaces. Ph.D. Thesis, Department of Aerospace Engineering, University of Minnesota, U.S.A.

Behr, M., Hastreiter, D., Mittal, S. & Tezduyar, T. E. 1995 Incompressible flow past a circular cylinder: dependence of the computed flow field on the location of the lateral boundaries. *Computer Methods in Applied Mechanics and Engineering* **123,** 309–316.

Behr, M., Liou, J., Shih, R. & Tezduyar, T. E. 1991 Vorticity-stream function formulation of unsteady incompressible flow past a cylinder: sensitivity of the computed flow field to the location of the outflow boundary. *International Journal for Numerical Methods in Fluids* **12,** 323–342.

Chen, Y. M., Ou, Y. R. & Pearlstein, A. J. 1993 Development of the wake behind a circular cylinder implulsively started into rotary and rectilinear motion. *Journal of Fluid Mechanics* **253,** 449–484.

Chew, Y. T., Cheng, M. & Luo, S. C. 1995 A numerical study of flow past a rotating circular cylinder using a hybrid vortex scheme. *Journal of Fluid Mechanics* **299,** 35–71.

Chew, Y. T., Pan, L. S. & Lee, T. S. 1998 Numerical simulation of the effect of a moving wall on separation of flow past a symmetrical aerofoil. *Proceedings of the Institution of Mechanical Engineers* **212,** 69–77.

Coutanceau, M. & Menard, C. 1985 Influence of rotation on the near-wake development behind an impulsively started circular cylinder. *Journal of Fluid Mechanics* **158,** 399–446.

Franca, L. P. & Frey, S. L. 1992 Stabilized finite element methods: II. The incompressible Navier–Stokes equations. *Computer Methods in Applied Mechanics and Engineering* **99,** 209–233.

Franca, L. P., Frey, S. L. & Hughes, T. J. R. 1992 Stabilized finite element methods: I. Application to the advective–diffusive model. *Computer Methods in Applied Mechanics and Engineering* **95,** 253–276.

Gad-El-Hak, M. & Bushnell, D. M. 1991 Separation control: Review. *ASME Journal of Fluids Engineering* **113,** 5–29.

Goldstein, S. 1938 *Modern Developments in Fluid Dynamics.* Oxford: Clarendon Press.

Griffin, O. M. & Hall, M. S. 1991 Review-vortex shedding lock-on and flow control in bluff body wakes. *ASME Journal of Fluids Engineering* **113,** 526–537.

Hughes, T. J. R. & Brooks, A. N. 1979 A multi-dimensional upwind scheme with no crosswind diffusion. In *Finite Element Methods for Convection Dominated Flows* (ed. T. J. R. Hughes), AMD-Vol.34, pp. 19–35. New York: ASME.

Hughes, T. J. R. & Tezduyar, T. E. 1984 Finite element methods for first-order hyperbolic systems with particular emphasis on the compressible Euler equations. *Computer Methods in Applied Mechanics and Engineering* **45,** 217–284.

Lecointe, Y., Piquet, J., & Plantec, J. 1987 Flow structure in the wake of an oscillating cylinder. In *Forum on Unsteady Flow Separation* (ed. K. N. Ghia), FED-52, pp. 147–157. New York: ASME.

Mittal, S. 1992 Stabilized space–time finite element formulations for unsteady incompressible flows involving fluid–body interactions. Ph.D. Thesis, University of Minnesota, U.S.A.

Mittal, S. 2000*a* On the performance of high aspect-ratio elements for incompressible flows. *Computer Methods in Applied Mechanics and Engineering*. **188**, 269–287.

Mittal, S. 2000*b* Reduction of unsteady forces on bluff bodies using rotating control cylinders. In *IUTAM-Symposium on Mechanics of Passive and Active Flow Control* (eds G. E. A. Meier & P. R. Viswanath). Dordrecht: Kluwer Academic Publishers.

Mittal, S. & Tezduyar, T. E. 1992 A finite element study of incompressible flows past oscillating cylinders and airfoils. *International Journal for Numerical Methods in Fluids* **15,** 1073–1118.

Mittal, S. & Kumar, V. 1999 Finite element study of vortex-induced cross-flow and in-line oscillations of a circular cylinder at low Reynolds numbers. *International Journal for Numerical Methods in Fluids* **31,** 1087–1120.

Mittal, S. & Kumar, V. 2000 Flow induced vibrations of a light circular cylinder at Reynolds numbers 10^3 to 10^4. *Journal of Sound and Vibration* (Submitted).

Mittal, S., Kumar, V. & Raghuvanshi, A. 1997*a* Unsteady incompressible flow past two cylinders in tandem and staggered arrangements. *International Journal for Numerical Methods in Fluids* **25,** 1315–1344.

MITTAL, S., NAIR, M. T. & SENGUPTA, T. K. 1997*b* Numerical simulation of flow past rotating & translating circular cylinder. In *Proceedings of the Seventh Asian Congress of Fluid Mechanics*, pp. 701–704, Indian Institute of Technology Madras, Chennai, India. New Delhi, India: Allied Publishers Limited.

MITTAL, S. & RAGHUVANSHI, A. 2000 Control of vortex shedding behind circular cylinder for flow at low Reynolds numbers. *International Journal for Numerical Methods in Fluids* (to appear).

MITTAL, S. & TEZDUYAR, T. E. 1995 Parallel finite element simulation of 3D incompressible flows: fluid–structure interactions. *International Journal for Numerical Methods in Fluids* **21,** 933–953.

MODI, V. J. 1997 Moving surface boundary-layer control: a review. *Journal of Fluids and Structure* **11,** 627–663.

MODI, V. J., FERNANDO, M. S. U. K. & YOKOMIZO, T. 1991*a* Moving surface boundary-layer control: studies with bluff bodies and applications. *AIAA Journal* **29,** 1400–1406.

MODI, V. J., MOKHTARIAN, F. & FERNANDO, M. S. U. K. 1991*b* Moving surface boundary-layer control as applied to two-dimensional airfoils. *Journal of Aircraft* **28,** 104–112.

MODI, V. J., MUNSHI, S. R. & YOKOMIZO, T. 2000 Moving surface boundary-layer control as applied to slender and bluff bodies. *IUTAM-Symposium on Mechanics of Passive and Active Flow Control* (eds G. E. A. Meier & P. R. Viswanath). Dordrecht: Kluwer Academic Publishers.

MODI, V. J., SHIH, E., YING, B. & YOKOMIZO, T. 1992 Drag reduction of bluff bodies through momentum injection. *Journal of Aircraft* **29,** 429–436.

MUNSHI, S. R., MODI, V. J. & YOKOMIZO, T. 1997*a* Control of fluid-structure interaction instabilities through momentum injection. In *Proceedings of the Seventh Asian Congress of Fluid Mechanics*, pp. 335–338, Indian Institute of Technology Madras, Chennai, India. New Delhi, India: Allied Publishers Limited.

MUNSHI, S. R., MODI, V. J. & YOKOMIZO, T. 1997*b* Aerodynamics and dynamics of rectangular prisms with momentum injection. *Journal of Fluids and Structures* **11,** 873–892.

ONGOREN, A. ROCKWELL, D. 1988*a* Flow structure from an oscillating cylinder, Part 1. Mechanisms of phase shift and recovery in the near wake. *Journal of Fluid Mechanics* **191,** 197–223.

ONGOREN, A. & ROCKWELL, D. 1988*b* Flow structure from an oscillating cylinder. Part 2. Mode competition in the near wake. *Journal of Fluid Mechanics* **191,** 225–245.

SAAD, Y. & SCHULTZ, M. 1986 GMRES: a generalized minimal residual algorithm for solving nonsymmetric linear systems. *SIAM Journal of Scientific and Statistical Computing* **7,** 856–869.

SHAKIB, F. & HUGHES, T. J. R. 1991 A new finite element formulation for computational fluid dynamics: IX. Fourier analysis of space–time Galerkin/least-squares, algorithms. *Computer Methods in Applied Mechanics and Engineering* **87,** 35–58.

STRYKOWSKI, P. J. & SREENIVASAN, K. R. 1990 On the formation and suppression of vortex 'shedding' at low Reynolds numbers. *Journal of Fluid Mechanics* **218,** 71–107.

TEZDUYAR, T. E., MITTAL, S., RAY, S. E. & SHIH, R. 1992 Incompressible flow computations with stabilized bilinear and linear equal-order-interpolation velocity-pressure elements. *Computer Methods in Applied Mechanics and Engineering* **95,** 221–242.

TOKUMARU, P. T. & DIMOTAKIS, P. E. 1991 Rotary oscillation control of cylinder wake. *Journal of Fluid Mechanics* **224,** 77–90.

TOKUMARU, P. T. & DIMOTAKIS, P. E. 1993 The lift of a cylinder executing rotary motions in a uniform flow. *Journal of Fluid Mechanics* **255,** 1–10.

WILLIAMSON, C. H. K. & ROSHKO, A. 1988 Vortex formation in the wake of an oscillating cylinder. *Journal of Fluids and Structures* **2,** 355–381.

ZDRAVKOVICH, M. M. 1981 Review and classification of various aerodynamic and hydrodynamic means for suppressing vortex shedding. *Journal of Wind Engineering and Industrial Aerodynamics* **7,** 145–189.